JPET Fast Forward. Published on August 6, 2012 as DOI:10.1124/jpet.112.196097

Activation of Alternate Pro-Survival Pathways Accounts for Acquired Sunitinib Resistance in U87MG Glioma Xenografts

Qingyu Zhou, Hua Lv, Amin R. Mazloom, Huilei Xu, Avi Ma'ayan, James M. Gallo

Department of Pharmacology and Systems Therapeutics, Systems Biology Center New York, Mount Sinai School of Medicine, New York, NY 10029. (Q.Z., H.L., A.R.M., H.X, A.M., J.M.G)

Running title: Activated pro-survival pathways in sunitinib resistant tumor

Corresponding author: Qingyu Zhou

Current address: Department of Pharmaceutical Sciences, College of Pharmacy, University of South Florida, Tampa, FL 33612. E-mail: qzhou1@health.usf.edu

Number of text pages: 37.

Number of tables: 2.

Number of figures: 5.

Number of references: 47.

Number of words in the Abstract: 250.

Number of words in the Introduction: 676.

Number of words in the Discussion: 1486.

Nonstandard abbreviations: ANOVA, one-way analysis of variance; AUC, area under the curve; BH, Benjamini–Hochberg; c-Jun, Jun proto-oncogene; DAG, diacylglycerol; DMEM, Dulbecco's modified Eagle's medium; ERK1/2, extracellular signal-regulated kinase 1/2; GSK3α/β, glycogen synthase kinase 3α/β; HPBCD, 2-hydroxypropyl-β-cyclodextrin; IF, interstitial fluid; IL, interleukin; IP3, inositol 1,4,5- trisphosphate; JNK, c-Jun NH_2-terminal kinase; MAP, mitogen-activated protein; MMP, matrix metallopeptidase; NG2, neurogenin 2 chondroitin sulfate proteoglycan; NIH, National Institute of Health; PBS, phosphate buffered saline; PCA, Principal component analysis; PCR, polymerase chain reaction; PDGFR, platelet-derived growth factor receptor; PK, pharmacokinetic; PLC-γ1, phospholipase *C*-γ1; RCC, renal cell carcinoma; RTK, receptor tyrosine kinase; α-SMA, α-smooth muscle actin; STAT5α/β, signal transducers and

activators of transcription 5α/β; VEGF, vascular endothelial growth factor; VEGFR, vascular endothelial growth factor receptors.

Recommended Section: Chemotherapy, Antibiotics, and Gene Therapy

Abstract

Acquired drug resistance represents a major obstacle to using sunitinib for the treatment of solid tumors. Here, we examined the cellular and molecular alterations in tumors that are associated with acquired brain tumor resistance to sunitinib using an *in vivo* model. U87MG tumors obtained from nude mice that received sunitinib 40 mg/kg/day for 30 days were classified as sunitinib-sensitive and -resistant groups based on tumor volume and underwent targeted gene microarray and protein array analyses. The expression of several angiogenesis-associated genes was significantly modulated in sunitinib-treated tumors compared with those in control tumors ($p < 0.05$), whereas no significant differences were observed between sunitinib-sensitive and –resistant tumors ($p > 0.05$). Tumor vasculature based on microvessel density, neurogenin 2 chondroitin sulfate proteoglycan (NG2) density and α-smooth muscle actin (α-SMA) density was also similar in sunitinib-treatment groups ($p > 0.05$). The moderate increase in unbound sunitinib tumor-to-plasma area-under-the-curve (AUC) ratio in sunitinib-resistant mice was accompanied by upregulated ABCG2 expression in tumor. The most profound difference between sunitinib-sensitive and –resistant groups was found in the expression of several phosphorylated proteins involved in intracellular signaling. In particular, phospholipase *C*-γ1 (PLC-γ1) phosphorylation in sunitinib-resistant tumors was upregulated by 2.6 folds compared with that in sunitinib-sensitive tumors ($p < 0.05$). In conclusion, acquired sunitinib resistance in U87MG tumors is not associated with revascularization in tumors, but rather with activation of alternate pro-survival pathways involved in an escape mechanism facilitating tumor growth and possibly insufficient drug uptake in tumor cells due to an upregulated membrane efflux transporter.

Introduction

The concept that sustained angiogenesis is an essential feature of many human cancers has rendered the inhibition of tumor angiogenesis a promising strategy for cancer treatment [Hanahan and Weinberg, 2000]. The finding of vascular endothelial growth factor (VEGF) as a key mediator of angiogenesis in cancer was a milestone that spurred appreciable research efforts to develop therapeutic agents selectively targeting VEGF ligands and their receptors [Leung *et al*., 1989; Ferrara *et al*., 2004]. In spite of impressive preclinical results and initial positive responses of patients, anti-VEGF therapy has yet to show an overall survival benefit and most patients eventually relapse due to the acquisition of drug resistance [Shojaei and Ferrara, 2007]. The postulated resistance mechanisms are diverse and as such attest to the challenge of devising treatment strategies that might prevent drug resistance [Bergers and Hanahan, 2008; Azam *et al*., 2010].

Acquired tumor resistance to antiangiogenic therapy occurs after treatment with selective inhibitors targeting VEGF receptors [Casanovas *et al*., 2005; Lucio-Eterovic *et al*., 2009] as well as other multitargeted antiangiogenic agents, such as sunitinib. Sunitinib is a small-molecule multi-kinase inhibitor having antiangiogenic and antitumor activities achieved through the inhibition of several related receptor tyrosine kinases (RTKs), including vascular endothelial growth factor receptors 1-3 (VEGFR1-3), platelet-derived growth factor receptor α and β (PDGFR α/β), stem cell factor receptor and FMS-like tyrosine kinase 3 [Sun *et al*., 2003; Mendel *et al*., 2003]. Despite initial reports suggesting clinical efficacy in various types of solid tumors [George 2007; Motzer *et al*., 2006; Liljegren *et al*., 2009], acquired resistance to sunitinib has emerged as a major obstacle for improving overall response rate and survival of cancer patients. Even though there is an urgent need to understand the mechanisms underlying acquired sunitinib resistance, only a handful of experimental studies have been performed to date. A diversity of mechanisms underlying the sunitinib resistance phenotype has been

elucidated under different experimental conditions, including various *in vitro* and/or *in vivo* approaches utilizing different tumor cell lines [Yang *et al*., 2012; Kutikov *et al*., 2011; Bender and Ullrich, 2011; Huang *et al*., 2010; Gotink *et al*., 2011]. Each individual study has focused merely on one aspect of resistance, either a distinct proangiogenic factor, a pro-survival signaling pathway [Yang et al., 2012; Kutikov *et al*., 2011; Bender and Ullrich, 2011; Huang *et al*., 2010], or lysosomal sequestration [Gotink *et al*., 2011]; thus, in-depth knowledge about the mechanisms involved in acquired sunitinib resistance is still lacking.

Brain tumor chemotherapy also suffers from the development of acquired drug resistance and in addition, due to the presence of the blood-brain barrier can negatively impact drug penetration, and might be considered an intrinsic resistance factor. Nonetheless, a recent study demonstrated the potent antiangiogenic and anti-invasive effects of sunitinib on experimental human glioblastomas using mouse brain slices implanted with GL15 glioblastoma cells or fresh human glioma biopsy specimens [de Boüard *et al*., 2007], and thus, provided a rationale of using sunitinib for patients with malignant gliomas. Currently, a phase II trial of sunitinib in patients with recurrence malignant gliomas is underway at the National Institute of Health (NIH) (http://clinicaltrials.gov/ct2/show/NCT00923117). In light of the potential use of sunitinib for the treatment of brain cancer and possible occurrence of sunitinib resistance over time, additional knowledge about the molecular alterations and features of brain tumors in relation to tumor resistance to sunitinib would be essential for the design of effective drug combinations that may maximize patient responses. The aim of this study was to identify pharmacokinetic (PK), cellular and molecular alterations in gliomas that are associated with phenotypic resistance to sunitinib. To accomplish this, an *in vivo* drug resistance tumor model was established based on the differential growth of subcutaneous tumors in mice to determine the role of both cellular and vascular components in the acquisition of sunitinib resistance. The expression levels of angiogenesis markers and angiogenesis-associated genes in tumors were measured as well as

the phosphorylation levels of various proteins that regulate various pro-survival signaling pathways in the sensitive and resistant phenotypes. This approach enabled us to provide a broader understanding of sunitinib resistance.

Materials and Methods

Materials

Sunitinib malate (Sutent®. N-[2-(Diethylamino)ethyl]-5-[(Z)-(5-fluoro-1,2-dihydro-2-oxo-3H-indol-3-ylidene)methyl]-2,4-dimethyl-1H-pyrrole-3-carboxamide (2S)-2-hydroxybutanedioic acid (1:1) salt) was purchased from LC Laboratories (Woburn, MA) and dissolved in deionized water at a stock concentration of 5.35 mg/ml (= 4 mg of sunitinib base per ml). All other chemicals, solvents and reagents were obtained from commercial sources.

Male NIH Swiss nude mice (*nu*/*nu*, 6-7 weeks old) were purchased from Taconic Farms (Germantown, NY). All animal experiments were approved by the Institutional Animal Care and Use Committee and performed according to the NIH guidelines.

U87MG human glioma cells were purchased from the American Type Culture Collection and cultured in Dulbecco's modified Eagle's medium (DMEM) supplemented with 10% fetal bovine serum, 100 units/ml penicillin and 100 µg/ml streptomycin, and maintained in a humidified atmosphere of 5% CO_2 in air at 37^{o}C.

Sunitinib-Sensitive and –Resistant Xenograft Tumor Model

U87MG cells (5×10^6) suspended in 0.2 ml Matrigel (BD Biosciences) were inoculated subcutaneously in the dorsal neck region of the nude mice. Tumor growth was monitored once a week with the volume calculated as $0.5 \times \text{length} \times \text{width}^2$. Tumor engraftment and growth was observed in all animals 14 days after tumor implantation. Tumor-bearing mice were randomized into two groups to initiate treatment; vehicle control (N = 5) and 40 mg/kg sunitinib group (N = 21), based on tumor volume. Each mouse received oral once-daily administration of either vehicle or sunitinib with a 6-day-on and 1-day-off doing schedule for 30 days. Phenotypic sensitivity of individual mice to sunitinib treatment was defined based on the degree of

suppression of tumor growth. Sunitinib-treated mice were classified into sunitinib-sensitive and –resistant groups according to the median value of fold change of tumor volume after the 30-day treatment period, which was calculated as the ratio of tumor volume on Day 30 to that on Day 0.

Pharmacokinetic Blood Sampling and Tumor Microdialysis

On Day 30, a subgroup of sunitinib-treated tumor-bearing mice that consisted of 6 sunitinib-sensitive and 4 sunitinib-resistant animals underwent PK measurements. The day before the last dose of sunitinib, the carotid artery of each mouse was catheterized for blood sampling [Zhou *et al*., 2008]. Blood samples were taken prior to, and at 5, 15 and 30 min, 1, 2, 3, 4, 6, 8 and 24 h after sunitinib administration on Day 30. Plasma was separated by centrifugation and stored at -80 ^{o}C until analyzed for sunitinib. Tumor microdialysis was performed to determine unbound sunitinib concentrations in tumor interstitial fluid (IF). In brief, on the day of PK study, a CMA/20 Elite microdialysis probe with the membrane length of 4 mm and molecular weight cut-off of 20 kDa was inserted into the central region of the tumor and perfused with Ringer's solution containing 5% (w/v) 2-hydroxypropyl-β-cyclodextrin (HPBCD) at a flow rate of 0.6 µl/min. After the first 5 hours of sample collection after drug administration, dialysate samples were collected at different flow rates 0.6, 1.2, and 2 µL/min at a time interval of 30 min consistent with the zero flow rate calibration method as described in the supplementary methods [Elmeliegy *et al*., 2011].

Sunitinib concentrations in plasma and tumor IF were determined using a validated liquid chromatography tandem mass spectrometry (LC-MS/MS) method as previously reported [Zhou and Gallo, 2010].

Immunofluorescence Double Staining

Frozen subcutaneous tumor samples collected from the PK study were cryosectioned at 10 µm, fixed in 4% paraformaldehyde, and then blocked with 1.5% goat serum in phosphate

buffered saline (PBS). Sections were incubated overnight at 4°C in either a mixture of 1:400 rat anti-mouse CD31 (BD Pharmingen) and 1:200 rabbit anti-mouse α-SMA (Abcam) or a mixture of 1:400 rat anti-mouse CD31 and 1:200 rabbit anti-mouse NG2 (Millipore). After washed with PBS, tumor sections were incubated for 1 hour at room temperature in dark with a mixture of 1:200 Alexa Fluor 488 conjugated goat anti-rat IgG and 1:200 Alexa Fluor 568 conjugated goat anti-rabbit IgG (Invitrogen). Fluorescent immunostained sections were examined under a Zeiss Axioplan2IE fluorescence microscope with Zeiss HC PL Fluotar 10 and 20X/0.5 NA dry objective. Images were processed with MetaMorph 4.6-5 (Molecular Devices).

Angiogenesis Polymerase Chain Reaction (PCR) Array

Tumor samples obtained from another subgroup of sunitinib-treated animals, which were not recruited in the PK study and consisted of 4 sunitinib-sensitive and 7 sunitinib-resistant mice, were used in the angiogenesis real-time PCR arrays designed to determine the expression levels of genes involved in modulating the biological processes of angiogenesis in either humans or mice (SA Biosciences). Total RNA extracted from tumor tissues with Trizol reagent (Invitrogen) was converted to cDNA using random hexamer primers and AMV reverse transcription reagents as per the manufacturer's protocol (Promega). The cDNA samples were then subjected to the real-time PCR arrays. To visualize the results we subtracted the C_T values of angiogenesis genes from the GAPDH expression and then subtracted the mean and divided by the standard deviation across all samples (Z-score normalization). To identify differentially expressed genes across all groups the ANOVA was applied with Benjamini–Hochberg (BH) correction ($p < 0.05$). To identify differentially expressed genes between sensitive and resistant groups a *t*-test was used with the BH correction ($p < 0.05$). Principal component analysis (PCA) was applied to the expression vectors across all samples as well as to an average vector for each of the three groups; control, sunitinib-sensitive and –resistant.

Human Phospho-Kinase Antibody Array Study

Representative subcutaneous tumor samples from individual study groups (N = 4 from each group) were processed using the human phosphor-kinase array kit (ARY003, R&D Systems), which include 46 intracellular serine/threonine/tyrosine kinases according to the manufacturer's protocol. A qualitative assessment of the modulation effect of sunitinib on the expression of phosphorylated kinases was performed with the following two criteria: 1) A protein expression ratio of the sunitinib-treated tumor to the control tumor being ≥ 1.5 was considered upregulation; 2). A protein expression ratio of the control tumor to the sunitinib-treated tumor being ≥ 1.5 was considered downregulation.

Western Blot Analysis

Tumor lysate samples were prepared as previously described [Zhou *et al*., 2008] and subjected to immunoblotting with the following antibodies purchased from Cell Signaling: Jun proto-oncogene (c-Jun, 1:1000), phosphorylated c-Jun (p-c-Jun, 1:1000), extracellular signal-regulated kinase 1/2 (ERK1/2, 1:1000), phosphorylated ERK1/2 (p-ERK1/2, 1:1000), glycogen synthase kinase 3α/β (GSK3α/β, 1:1000), phosphorylated GSK 3α/β (p-GSK3α/β, 1:1000), phospholipase *C*-γ1 (PLC-γ1, 1:1000), phosphorylated PLC-γ1 (p-PLC-γ1, 1:1000), signal transducers and activators of transcription 5α/β (STAT5α/β, 1:1000) and phosphorylated STAT5α/β (p- STAT5α/β, 1:1000) . Blots were incubated with horseradish peroxidase–conjugated secondary antibodies (1:15,000; Santa Cruz) and immunoreactive protein bands were visualized by the enhanced chemiluminescence system (PerkinElmer). Band areas were quantified by ImageJ software (from NIH and available at http://rsb.info.nih.gov/ij/). Normalization for loading differences was achieved by dividing the densitometry values for individual bands by the densitometry values for β-actin in the same lane. The expression levels

of individual proteins in sunitinib-treated tumors are presented as the percent change compared to those in the control tumors.

To measure the expression levels of ABCB1 and ABCG2, the crude membrane was extracted from individual tumor tissues as described in the supplementary methods and subjected to the Western blotting using the ABCB1 (1:100, Calbiochem) and ABCG2 antibodies (1:500, Santa Cruz) following the same abovementioned protocol.

Statistical Analyses

Except for the real-time PCR array data, data analyses were performed using Number Cruncher Statistical Systems 2007 (Keysville, UT). Data are presented as the mean ± standard deviation (SD). Comparison of means between two independent groups was made using the Mann-Whitney U test. Comparison of means among three study groups was made using one-way analysis of variance (ANOVA) followed by the post-hoc Tukey-Kramer Multiple-Comparison Test. Spearman's rank correlation was used to describe relations between two variables. A two-sided *p*-value of less than 0.05 was considered statistically significant.

Results

Inhibitory Effect of Sunitinib on Tumor Growth

Significant suppression of tumor growth in sunitinib treatment groups was observed on Day 9 and Day 16 ($p < 0.01$ for both as compared with the vehicle control). Vehicle-treated mice were sacrificed 16 days after the initiation of the treatment due to their tumors reaching the allowed maximum size (2000 mm^3). Sunitinib-treated mice exhibited different tumor growth rates during the 30-day treatment period. The fold change of tumor volume after the 30-day treatment period ranged from 0.7 – 11.5 with the median value of 4.7. This median value was then used as the cut-off point to classify sunitinib-treated mice into sunitinib-sensitive and –resistant groups (Fig. 1A; Supplementary Table S1). Significant differences in mean tumor volume (Supplementary Figure S1) and tumor volume ratio (*i.e*., the ratio of tumor volume measured at an indicated time to tumor volume at the start of vehicle or sunitinib treatment) (Fig. 1B) between the sunitinib-sensitive and –resistant groups were observed on Day 23 and Day 30 ($p < 0.01$ for both), indicating that sunitinib exhibits greater antitumor efficacy in sunitinib-sensitive mice than in sunitinib-resistant mice.

Sunitinib Pharmacokinetic Study in Sunitinib-Sensitive and –Resistant Mice

The PK study was performed to determine if the reduced effectiveness of sunitinib was attributable to insufficient drug penetration into tumor cells. The unbound sunitinib plasma AUC was calculated based on the reported sunitinib unbound fraction value of 9% in the mouse plasma [Haznedar *et al*., 2009]. Although there were trends of altered PK characteristics (*i.e.* decreased unbound plasma AUC and increased clearance) in the sunitinib-resistant group (Table 1), the differences were insignificant compared to the sunitinib-sensitive group ($p > 0.05$). Nonetheless, a 19% increase in the mean unbound sunitinib tumor IF to plasma AUC ratio in the sunitinib-resistant group compared with that in the sunitinib-sensitive group raised

speculation that activated efflux pumps in the plasma membrane of tumor cells efflux drug from the intracellular space to the interstitial space.

Evaluation of Tumor Angiogenesis in Sunitinib-Sensitive and –Resistant Tumors

Pericytes on tumor blood vessels express distinct markers at different stages of differentiation [Morikawa *et al*., 2002]. NG2 proteoglycan is a cell surface molecule and a prominent component of pericytes in tumor microvessels. It has the potential to affect tumor progression by contributing to pericyte recruitment and to pericyte–endothelial cell interactions [Ozerdem *et al*., 2002; Brekke *et al*., 2006]. In contrast, α-SMA has been reported as a marker of mature mural cells including both pericytes and smooth muscle cells [Yonenaga *et al*., 2005]. In this study, sunitinib treatment significantly reduced the tumor microvessel density and pericyte recruitment as indicated by the CD31 and NG2 immunostaining ($p < 0.01$ for both, Fig. 2A and 2C). Sunitinib had no effect on the α-SMA density, but significantly increased the number of α-SMA positive cells lining CD31-positive endothelial cells relative to the total number of CD31-positive endothelial cells, which is reflected by the percentage of α-SMA/CD31 double-positive structures ($p < 0.01$ for both sunitinib-resistant and –sensitive tumors; Fig. 2B and 2D) and considered an index of vessel maturation [Djokovic *et al*., 2010]. The mean percentage of CD31-positive structures covered by NG2-positive area was significantly reduced in both sunitinib-sensitive and –resistant tumors as compared with that in the control tumors ($p < 0.05$ and 0.01 for sunitinib- sensitive and – resistant tumors, respectively, Fig. 2A and 2C), suggesting markedly impaired pericyte recruitment, and also indicates reduced new blood vessel formation in tumors. Overall the results suggest that sunitinib targets mainly newly formed immature tumor vessels thereby increasing the proportion of functional vessels in tumors. No significant differences were found between sunitinib-sensitive and –resistant groups in tumor microvessel density, NG2 density, α-SMA density and the percentage of either α-SMA/CD31 or NG2/CD31 double-positive structures. This implies that even though tumor

angiogenesis is inhibited to the same extent in both sunitinib-sensitive and –resistant tumors, alternative pro-survival pathways that allow tumor growth to be less dependent on tumor neovascularization may be activated to a greater degree in the resistant tumors compared with those in the sensitive tumors.

Angiogenesis Polymerase Chain Reaction Array

The species specific detection of the expression levels of human and mouse angiogenesis-associated genes was carried out using a real-time PCR array. The C_T values for individual genes are presented in Supplementary Tables S2 and S3. The unsupervised hierarchical bi-clustering approach was used to organize and explore the data and highlight groups of samples with similar gene expression patterns. Hierarchical clustering using the normalized C_T values generated two distinct clusters for both mouse and human angiogenesis-related genes. Cluster 1 contained all vehicle control animals (N = 5), and cluster 2 contained all sunitinib-treated animals, including 4 sunitinib-sensitive and 7 resistant animals (Fig. 3A and 3B). Likewise, principal component analysis (PCA) demonstrated that sunitinib-sensitive and –resistant groups displayed overall similar expression patterns for both human and mouse angiogenesis-associated genes, whereas the control group showed differential gene expression pattern compared with the two sunitinib treatment groups (Fig. 3C-3F). Moreover, 21 of the 84 mouse genes and 35 of the 84 human genes were differentially expressed between the control tumors and either sunitinib-sensitive or –resistant tumors ($p < 0.05$, Fig. 3G and 3H). While most resistant and sensitive groups appear to be segregated into two distinct groups by visually inspecting the hierarchical clustering and PCA plots, no significantly differentially expressed genes were found. Hence, the difference in the expression levels of either mouse or human genes was not significant between sunitinib-sensitive and –resistant groups, suggesting similar patterns of angiogenesis-related gene expression in the sunitinib-sensitive and –resistant tumors.

Human Phospho-Kinase Antibody Array Study

Even though the results of both immunostaining and angiogenesis PCR array showed that tumor angiogenesis was inhibited to a similar degree in both sunitinib-sensitive and –resistant tumors, the relatively rapid growth rate of sunitinib-resistant tumors suggests that there are potentially cell signaling pathways that differentially regulate tumor cell proliferation and survival in the resistant tumors. Since pro-survival signaling pathways are known to play an important role in drug resistance, a human phosphor-kinase antibody array was used to screen for potential markers for the acquisition of sunitinib resistance. Fig. 4A and 4B show the fold changes in protein expression of phosphorylated kinases and their substrates that were either upregulated (≥ 1.5, sunitinib-treated to control) or downregulated (≥ 1.5, control to sunitinib-treated), respectively. A network diagram depicting the relationships between these proteins and their substrates in the context of cell signaling pathways is shown in Fig. 4C and 4D; however it should be viewed as the definitive network since there are many other regulators involved that are not shown. In addition, the references for the links between components are from different cell types, being either human or mouse. However, it can be seen that the upregulated proteins in the resistant tumors and the down-regulated proteins in the sensitive tumors form a pathway that can mediate the phosphorylation of ERK1/2, which subsequently upregulates c-Jun expression, as well as another set of transcription factors, STAT5α/β. Moreover, the upregulation of GSK3α/β is also likely to play a role in the activation of c-Jun suggesting a coherent feed-forward network motif amongst effectors of c-Jun in sunitinib-resistant tumors.

Western Blot Analysis

Based on the phosphor-kinase antibody array results, semi-quantitative Western blot analyses were conducted to confirm that the following proteins were upregulated in the

sunitinib-resistant tumors: ERK1/2 (T202/Y204), GSK3α/β (S21/S9), PLCγ-1 (Y783), c-Jun (S63), STAT5α/β (Y699). As shown in Fig. 5B and 5C, the expression levels of p-PLC-γ1 ($P < 0.01$), total PLC-γ1 ($p < 0.05$) and total c-Jun ($p < 0.05$) in the sunitinib-resistant tumor were significantly upregulated compared with those in the control tumors. The expression level of p-PLC-γ1 and total GSK3β in sunitinib-resistant tumors was significantly higher than that in sunitinib-sensitive tumors ($p < 0.05$ and 0.01 for total GSK3β and p-PLC-γ1, respectively). Expression of p-c-Jun appeared to be upregulated in the sunitinib-resistant tumors but down-regulated in the sensitive tumors, and the difference between those two groups was significant ($p < 0.05$). Differences in the expression levels of p-ERK1/2, total ERK, p-GSK3α/β, and total GSK3α among the three study groups were not statistically significant (Fig. 5C). The expression levels of phosphorylated and total STAT5α/β were not detectable by the Western blotting analysis. To examine whether the expression of the tested proteins would be associated with tumor growth following sunitinib treatment, the expression levels of individual proteins were compared with tumor volume on Day 30 or fold changes of tumor volume after the 30-day treatment period using Spearman correlation coefficients. Since the relationship between any two variables might be linear or log-linear, rank-based coefficients, such as Spearman's coefficients, would yield more robust estimates of correlation than linear coefficients, such as Pearson's coefficients, which could be strongly biased by extreme values. Using Spearman correlation analyses, the fold change of tumor volume was found to be significantly correlated with p-PLC-γ1 ($r = 0.636$, $p = 0.048$; Supplementary Figure S2A), total ERK1/2 ($r = 0.661$, $p = 0.038$; Supplementary Figure S2B), and total GSK3β ($r = 0.636$, $p = 0.048$; Supplementary Figure S2C).

Sunitinib is known to be a substrate [Tang *et al*., 2012] and inhibitor [Shukla *et al*., 2009] of ABCG2, a membrane transporter that serves as a drug efflux pump. In this study, the ABCG2 expression levels in tumors appeared to be upregulated in both sunitinib-sensitive (by 36%) and

–resistant (by 72%) tumors as compared with that in the control tumors although only the difference between the sunitinib-resistant and control groups was statistically significant ($p < 0.05$, Fig. 5C). This result suggests that the upregulation of ABCG2 in tumor cells may contribute to the acquired tumor resistance to sunitinib treatment. However, significant correlations were not found between tumor ABCG2 expression levels and either unbound sunitinib tumor or plasma AUC values or the tumor-to-plasma AUC ratios. The expression level of ABCB1 was not detected by the Western blot in all tumor samples.

Discussion

Efforts to identify mechanisms of sunitinib resistance in various cancer types have begun but none have focused on gliomas [Yang *et al*., 2012; Kutikov *et al*., 2011; Bender and Ullrich, 2011; Huang *et al*., 2010; Gotink *et al*., 2011]. In this study, a U87MG xenograft model was used to explore the potential mechanism involved in acquired sunitinib resistance. In contrast to *in vitro* models, the subcutaneous glioma model used here has the advantage of flexibility of treatment duration and direct assessment of a resistant phenotype based on tumor size, yet suffers a drawback of not capturing the native environment of brain tumors. Nonetheless, this study provides a framework for understanding the sequence of biologically programmed events in brain tumors leading to acquired sunitinib resistance.

In this study, sunitinib-treated animals were classified into to sunitinib-sensitive and resistant groups based on the median value of fold change of tumor volume after the 30-day treatment period (Fig. 1). Although the designation of sensitive and resistant groups is partially arbitrary, having two phenotypically distinct groups aids in characterizing differences in sunitinib-induced cellular and molecular alterations in tumor as well as in sunitinib's PK behavior. A similar approach was reported by Huang *et al.* [2010], who defined the sunitinib-resistant renal cell carcinoma (RCC) xenografts as those with more than 25% increase in the initial tumor volume, whereas those with the initial tumor volume increase being less than 25% were considered sunitinib-sensitive.

Consistent with the early study showing that sunitinib significantly reduced blood vessel formation but had little effect on existing blood vessels [Osusky *et al*., 2004], the double immunofluorescent staining results of this study suggest that the immature tumor vessels are more susceptible to sunitinib, while mature vessels are relatively resistant to it (Fig. 2). The remaining mature vessels in the tumors are able to maintain blood flow and provide oxygen and

nutrients, thereby supporting tumor growth [Jain 2001], which explains the observed gradually increased tumor volume in all sunitinib-treated animals in this study. Since there was no difference in tumor angiogenesis, measured in terms of microvessel density, pericyte density and percent of microvessel with pericyte coverage, between sunitinib-sensitive and –resistant groups, it is unlikely that the relatively rapid growth observed in sunitinib-resistant tumors is due to the restoration of sprouting tumor angiogenesis.

Resistance to antiangiogenic therapy in cancer involves both tumor cells and stromal components [Casanovas, 2011]. Although a human tumor xenograft in a mouse background is a mixture of human and mouse tissues, most studies on antiangiogenic drug resistance that included gene expression analyses of tumor xenografts have only determined human genes [Casanovas *et al*., 2005; Huang *et al*., 2010; Zhang *et al*., 2011]. In this study, the real-time PCR array assay was performed to obtain species-specific gene expression profiles. This enabled us to distinguish between angiogenesis-associated factors derived from human tumor cells and those from the mouse stroma, and thus, gain insight into tumor-stromal interactions related to the acquisition of sunitinib resistance. In line with findings of the immunohistochemistry study, results of the real-time PCR array demonstrated that the expression patterns of both human and mouse angiogenesis-related genes were different between control and sunitinib treatment groups, but not between sunitinib-sensitive and –resistant groups. However, the directed angiogenesis arrays would not have captured genes related to other resistant mechanisms. For example, in recent studies treatment with antiangiogenic agents has been demonstrated to increase local invasion and accelerate metastases [Pàez-Ribes *et al*., 2009; Ebos *et al*., 2009]. In this regard, whole genome-wide expression analysis would be necessary to locate likely differences not captured in the scope of this study which focused on tumor neovascularization. Nonetheless, several differentially expressed genes observed in this study were also reported by other research groups. For

example, Finke *et al.* [2011] reported that sunitinib-persistent myeloid derived suppressor cells (MDSCs) in metastatic RCC were associated with the upregulated expression of intratumoral matrix metallopeptidase 9 (MMP9), matrix metallopeptidase 8 (MMP8) and interleukin 8 (IL-8). In a preclinical study by Huang *et al.* [2010], plasma IL-8 levels were higher in sunitinib-resistant mice compared with those in sunitinib-sensitive mice. In the present study, the expression levels of *Mmp9* and *IL8* were significantly upregulated in sunitinib-treated tumors compared with control tumors. However, no difference was found between sunitinib-sensitive and resistant tumors (Fig. 3G and 3H). The discrepancy between findings of this study and those of Finke *et al*. [2011] and Huang *et al.* [2010] may be due to differences in study designs, including various tumor model used, different tissue sample examined and different treatment regimen applied.

The angiogenic array results revealed that the phenotypic resistance to sunitinib treatment was not attributed to the upregulation of alternative proangiogenic factors, which raised the question of whether modulation of other pro-survival pathways might contribute to the acquisition of sunitinib resistance. Using an antibody array followed by Western blotting verification, we identified a few differentially expressed kinase proteins in sunitinib-sensitive and –resistant tumors. There was some discrepancy between phosphor-kinase antibody arrays and Western blotting in terms of the magnitude of the fold changes, which is possibly attributable to the different efficacy of applied antibodies.

Results of the Western blot analysis showed that the expression levels of phosphorylated and total PLC-γ1 were elevated in sunitinib-sensitive and -resistant tumors compared with control tumors, but to a various degree. Moreover, the p-PLC-γ1 expression level in sunitinib-treated tumors was significantly correlated with the fold change of tumor volume ($p < 0.05$; Supplementary Figure S2A). The intracellular signaling molecule PLC-γ1 can be activated by various growth factors and hormones through their corresponding RTKs [Burgess *et al*., 1990; Kundra *et al*., 1994]. Activation of PLC-γ1 results in the formation of second messengers inositol

1,4,5- trisphosphate (IP3) and diacylglycerol (DAG), which subsequently mobilizes the release of calcium and activates protein kinase C isoforms, respectively, leading to diverse cellular responses. Phosphorylation on tyrosine residue 783 of PLC-γ1 is critical to its activation [Yu *et al*., 1998; Poulin *et al*., 2005]. A growing body of evidence has shown that PLC-γ1 promotes tumor invasion. For example, the PLCγ-1 expression in a metastatic tumor–derived head and neck squamous cell carcinoma (HNSCC) cell line was significantly upregulated compared with paired primary tumor–derived cell line. Treatment with the PLC inhibitor U73122 attenuated epidermal growth factor (EGF)-stimulated HNSCC invasion *in vitro* [Nozawa *et al*., 2008]. A mechanistic study using the MDA-MB-231 breast cancer cell line revealed that the phosphoinositide 3-kinase (PI3K) mediated activation of PLC-γ1 provided a link between integrin- and growth factor-mediated signaling pathways to regulate cell motility [Piccolo *et al*., 2002]. In this study, the upregulation of PLC-γ1 expression in sunitinib-treated tumors suggests that tumors change part of their molecular characteristics in response to sunitinib treatment to not only sustain tumor growth but also promote tumor invasion.

The expression of p-c-Jun was upregulated in the sunitinib-resistant tumors but down-regulated in the sensitive tumors (Fig. 5C). C-Jun and its upstream regulator c-Jun NH_2-terminal kinase (JNK) belong to one sub-group of mitogen-activated protein (MAP) kinases that can be stimulated by environmental stresses, cytokines and DNA-damaging agents [Weston and Davis, 2007]. The overexpression or activation of c-Jun appears to be antiapoptoic in various cancer cell lines, and targeting c-Jun increases the sensitivity of resistant cancer cells to DNA-damaging or microtubule-interacting agents [Pan *et al*., 2002; Obey *et al*., 2005; Duan *et al*., 2007]. In our case, the upregulation of phosphorylated and total c-Jun in addition to PLC-γ1 in sunitinib-resistant tumors indicates that more than one pro-survival pathway is activated in tumors resistant to sunitinib.

Tumor resistance to pharmaceutical intervention may be due to PK resistance that would culminate in lower intracellular drug exposure. In this study, upregulated ABCG2 expression level in sunitinib-treated tumors was associated with increased unbound tumor-IF-to-plasma AUC ratios. Sunitinib being a substrate of ABCG2 could be subjected to enhanced tumor cell efflux causing lower intracellular concentrations but higher concentrations in tumor IF. This interesting phenomenon that was detected *in vivo* by using tumor microdialysis has not been previously reported and offers an experimental approach to ascertain how intracellular drug concentrations may be altered by drug transport modulation. Even though no correlation was found between tumor ABCG2 expression levels and unbound sunitinib tumor-IF-to-plasma AUC ratios possibly due to a limited sample size, there is a sufficient basis to further study the role of ABCG2 in acquired sunitinib resistance.

In summary, based on the findings of this study, acquired tumor resistance to sunitinib is not associated with the revascularization in tumor, but associated with the activation of alternate pro-survival pathways, notably those mediated by PLC-γ1 and c-Jun proteins. The reduced drug uptake in tumor cells attributable to upregulated ABCG2 also appears to play a role in acquired sunitinib resistance. Further studies are needed to clarify the role of these potential resistance factors in sunitinib resistance; however without the use of an *in vivo* model of drug resistance that provides a foundation for further exploration including novel combination therapies, these leads are not likely to be identified.

Authorship Contributions

Participated in research design: Zhou and Gallo

Conducted experiments: Zhou and Lv.

Contributed new reagents or analytic tools: Lv.

Performed data analysis: Zhou, Mazloom, Xu, and Ma'ayan.

Wrote or contributed to the writing of the manuscript: Zhou, Xu, Ma'ayan and Gallo.

References:

Azam F, Mehta S, and Harris AL (2010). Mechanisms of resistance to antiangiogenesis therapy. *Eur J Cancer* **46**:1323-1332.

Bender C, and Ullrich A (2011). PRKX, TTBK2 and RSK4 expression causes sunitinib resistance in kidney carcinoma- and melanoma cell lines. *Int J Cancer* Oct 23. [Epub ahead of print].

Bergers G, and Hanahan D (2008). Modes of resistance to anti-angiogenic therapy. *Nat Rev Cancer* **8**:592–603.

Brekke C, Lundervold A, Enger PØ, Brekken C, Stålsett E, Pedersen TB, Haraldseth O, Krüger PG, Bjerkvig R, and Chekenya M (2006). NG2 expression regulates vascular morphology and function in human brain tumours. *Neuroimage* **29**:965-976.

Burgess WH, Dionne CA, Kaplow J, Mudd R, Friesel R, Zilberstein A, Schlessinger J, Jaye M (1990). Characterization and cDNA cloning of phospholipase C-gamma, a major substrate for heparin-binding growth factor 1 (acidic fibroblast growth factor)-activated tyrosine kinase. *Mol Cell Biol* **10**:4770-4777.

Casanovas O, Hicklin DJ, Bergers G, and Hanahan D (2005). Drug resistance by evasion of antiangiogenic targeting of VEGF signaling in late-stage pancreatic islet tumors. *Cancer Cell* **8**:299-309.

Casanovas O (2011). The adaptive stroma joining the antiangiogenic resistance front. *J Clin Invest* **121**:1244-1247.

de Boüard S, Herlin P, Christensen JG, Lemoisson E, Gauduchon P, Raymond E, and Guillamo JS (2007). Antiangiogenic and anti-invasive effects of sunitinib on experimental human glioblastoma. *Neuro Oncol* **9**:412-423.

Djokovic D, Trindade A, Gigante J, Badenes M, Silva L, Liu R, Li X, Gong M, Krasnoperov V, Gill PS, and Duarte A (2010). Combination of Dll4/Notch and Ephrin-B2/EphB4 targeted therapy is highly effective in disrupting tumor angiogenesis. *BMC Cancer* **10**:641.

Duan L, Sterba K, Kolomeichuk S, Kim H, Brown PH, and Chambers TC (2007). Inducible overexpression of c-Jun in MCF7 cells causes resistance to vinblastine via inhibition of drug-induced apoptosis and senescence at a step subsequent to mitotic arrest. *Biochem Pharmacol* **73**:481-490.

Ebos JM, Lee CR, Cruz-Munoz W, Bjarnason GA, Christensen JG, and Kerbel RS (2009). Accelerated metastasis after short-term treatment with a potent inhibitor of tumor angiogenesis. *Cancer Cell* **15**:232-239.

Elmeliegy MA, Carcaboso AM, Tagen M, Bai F, and Stewart CF (2011). Role of ATP-binding cassette and solute carrier transporters in erlotinib CNS penetration and intracellular accumulation. *Clin Cancer Res* **17**:89-99.

Ferrara N, Hillan KJ, Gerber HP, and Novotny W (2004). Discovery and development of bevacizumab, an anti-VEGF antibody for treating cancer. *Nat Rev Drug Discov* **3**:391-400.

Finke J, Ko J, Rini B, Rayman P, Ireland J, and Cohen P (2011). MDSC as a mechanism of tumor escape from sunitinib mediated anti-angiogenic therapy. *Int Immunopharmacol* **11**:856-861.

George S (2007). Sunitinib, a multitargeted tyrosine kinase inhibitor, in the management of gastrointestinal stromal tumor. *Curr Oncol Rep* **9**:323-327.

Hanahan D, and Weinberg RA (2008). The hallmarks of cancer. *Cell* **100**: 57–70.

Haznedar JO, Patyna S, Bello CL, Peng GW, Speed W, Yu X, Zhang Q, Sukbuntherng J, Sweeny DJ, Antonian L, and Wu EY (2009). Single- and multiple-dose disposition kinetics of sunitinib malate, a multitargeted receptor tyrosine kinase inhibitor: comparative plasma kinetics in non-clinical species. *Cancer Chemother Pharmacol* **64**:691-706.

Huang D, Ding Y, Zhou M, Rini BI, Petillo D, Qian CN, Kahnoski R, Futreal PA, Furge KA, and Teh BT (2010). Interleukin-8 mediates resistance to antiangiogenic agent sunitinib in renal cell carcinoma. *Cancer Res* **70**:1063-1071.

Gotink KJ, Broxterman HJ, Labots M, de Haas RR, Dekker H, Honeywell RJ, Rudek MA, Beerepoot LV, Musters RJ, Jansen G, Griffioen AW, Assaraf YG, Pili R, Peters GJ, and Verheul HM (2011). Lysosomal sequestration of sunitinib: A novel mechanism of drug resistance. *Clin Cancer Res* **17**:7337-7346.

Jain RK (2001). Normalizing tumor vasculature with anti-angiogenic therapy: a new paradigm for combination therapy. *Nat Med* **7**:987-989.

Kundra V, Escobedo JA, Kazlauskas A, Kim HK, Rhee SG, Williams LT, and Zetter BR (1994). Regulation of chemotaxis by the platelet-derived growth factor receptor-beta. *Nature* **367**:474-476.

Kutikov A, Makhov P, Golovine K, Canter DJ, Sirohi M, Street R, Simhan J, Uzzo RG, and Kolenko VM (2011). Interleukin-6: a potential biomarker of resistance to multitargeted receptor tyrosine kinase inhibitors in castration-resistant prostate cancer. *Urology* **78**:968.e7-11.

Leung DW, Cachianes G, Kuang WJ, Goeddel DV, and Ferrara N (1989). Vascular endothelial growth factor is a secreted angiogenic mitogen. *Science* **246**:1306-1309.

Liljegren A, Bergh J, and Castany R (2009). Early experience with sunitinib, combined with docetaxel, in patients with metastatic breast cancer. *Breast* **18**:259-262.

Lucio-Eterovic AK, Piao Y, and de Groot JF (2009). Mediators of glioblastoma resistance and invasion during antivascular endothelial growth factor therapy. *Clin Cancer Res* **15**:4589-4599.

Mendel DB, Laird AD, Xin X, Louie SG, Christensen JG, Li G, Schreck RE, Abrams TJ, Ngai TJ, Lee LB, Murray LJ, Carver J, Chan E, Moss KG, Haznedar JO, Sukbuntherng J, Blake RA, Sun L, Tang C, Miller T, Shirazian S, McMahon G, and Cherrington JM (2003). In vivo antitumor activity of SU11248, a novel tyrosine kinase inhibitor targeting vascular endothelial growth factor and platelet-derived growth factor receptors: determination of a pharmacokinetic/pharmacodynamic relationship. *Clin Cancer Res* **9**:327-337.

Morikawa S, Baluk P, Kaidoh T, Haskell A, Jain RK, and McDonald DM (2002). Abnormalities in pericytes on blood vessels and endothelial sprouts in tumors*. Am J Pathol* **160***:*985–1000.

Motzer RJ, Rini BI, Bukowski RM, Curti BD, George DJ, Hudes GR, Redman BG, Margolin KA, Merchan JR, Wilding G, Ginsberg MS, Bacik J, Kim ST, Baum CM, and Michaelson MD (2006). Sunitinib in patients with metastatic renal cell carcinoma. *JAMA* **295**:2516-2524.

Nozawa H, Howell G, Suzuki S, Zhang Q, Qi Y, Klein-Seetharaman J, Wells A, Grandis JR, and Thomas SM (2008). Combined inhibition of PLC{gamma}-1 and c-Src abrogates epidermal growth factor receptor-mediated head and neck squamous cell carcinoma invasion. *Clin Cancer Res* **14**:4336-4344.

Obey TB, Lyle CS, and Chambers TC (2005). Role of c-Jun in cellular sensitivity to the microtubule inhibitor vinblastine. *Biochem Biophys Res Commun* **335**:1179-1184.

Osusky KL, Hallahan DE, Fu A, Ye F, Shyr Y, and Geng L (2004). The receptor tyrosine kinase inhibitor SU11248 impedes endothelial cell migration, tubule formation, and blood vessel formation in vivo, but has little effect on existing tumor vessels. *Angiogenesis* **7**:225-233.

Ozerdem U, Monosov E, and Stallcup WB (2002). NG2 proteoglycan expression by pericytes in pathological microvasculature. *Microvasc Res* **63**:129-34.

Pàez-Ribes M, Allen E, Hudock J, Takeda T, Okuyama H, Viñals F, Inoue M, Bergers G, Hanahan D, and Casanovas O (2009). Antiangiogenic therapy elicits malignant progression of tumors to increased local invasion and distant metastasis. *Cancer Cell* **15**:220-231.

Pan B, Yao KS, Monia BP, Dean NM, McKay RA, Hamilton TC, and O'Dwyer PJ (2002). Reversal of cisplatin resistance in human ovarian cancer cell lines by a c-jun antisense oligodeoxynucleotide (ISIS 10582): evidence for the role of transcription factor overexpression in determining resistant phenotype. *Biochem Pharmacol* **63**:1699-1707.

Piccolo E, Innominato PF, Mariggio MA, Maffucci T, Iacobelli S, and Falasca M (2002). The mechanism involved in the regulation of phospholipase Cgamma1 activity in cell migration. *Oncogene* **21**:6520-6529.

Poulin B, Sekiya F, and Rhee SG (2005). Intramolecular interaction between phosphorylated tyrosine-783 and the C-terminal Src homology 2 domain activates phospholipase C-gamma1. *Proc Natl Acad Sci U S A* **102**:4276-4781.

Shojaei F, and Ferrara N (2007). Antiangiogenic therapy for cancer: an update. *Cancer J* **13**:345-348.

Shukla S, Robey RW, Bates SE, and Ambudkar SV (2009). Sunitinib (Sutent, SU11248), a small-molecule receptor tyrosine kinase inhibitor, blocks function of the ATP-binding

cassette (ABC) transporters P-glycoprotein (ABCB1) and ABCG2. *Drug Metab Dispos* **37**:359-365.

Sun L, Liang C, Shirazian S, Zhou Y, Miller T, Cui J, Fukuda JY, Chu JY, Nematalla A, Wang X, Chen H, Sistla A, Luu TC, Tang F, Wei J, and Tang C (2003). Discovery of 5-[5-fluoro-2-oxo-1,2- dihydroindol-(3Z)-ylidenemethyl]-2,4- dimethyl-1H-pyrrole-3-carboxylic acid (2-diethylaminoethyl)amide, a novel tyrosine kinase inhibitor targeting vascular endothelial and platelet-derived growth factor receptor tyrosine kinase. *J Med Chem* **46**:1116-1119.

Tang SC, Lagas JS, Lankheet NA, Poller B, Hillebrand MJ, Rosing H, Beijnen JH, and Schinkel AH (2012). Brain accumulation of sunitinib is restricted by P-glycoprotein (ABCB1) and breast cancer resistance protein (ABCG2) and can be enhanced by oral elacridar and sunitinib coadministration. *Int J Cancer* **130**:223-233.

Weston CR, and Davis RJ (2007). The JNK signal transduction pathway. *Curr Opin Cell Biol* **19**:142-149.

Yang J, Ikezoe T, Nishioka C, Takezaki Y, Hanazaki K, Taguchi T, and Yokoyama A (2012). Long-term exposure of gastrointestinal stromal tumor cells to sunitinib induces epigenetic silencing of the PTEN gene. *Int J Cancer* **130**:959-66.

Yonenaga Y, Mori A, Onodera H, Yasuda S, Oe H, Fujimoto A, Tachibana T, and Imamura M (2005). Absence of smooth muscle actin-positive pericyte coverage of tumor vessels correlates with hematogenous metastasis and prognosis of colorectal cancer patients. *Oncology* **69**:159-166.

Yu H, Fukami K, Itoh T, and Takenawa T (1998). Phosphorylation of phospholipase Cgamma1 on tyrosine residue 783 by platelet-derived growth factor regulates reorganization of the cytoskeleton. *Exp Cell Res* **243**:113-122.

Zhang L, Bhasin M, Schor-Bardach R, Wang X, Collins MP, Panka D, Putheti P, Signoretti S, Alsop DC, Libermann T, Atkins MB, Mier JW, Goldberg SN, and Bhatt RS (2011). Resistance of renal cell carcinoma to sorafenib is mediated by potentially reversible gene expression. *PloS One* **6**:e19144.

Zhou Q, Guo P, and Gallo JM (2008). Impact of angiogenesis inhibition by sunitinib on tumor distribution of temozolomide. *Clin Cancer Res* **14**:1540-1549.

Zhou Q, and Gallo JM (2010). Quantification of sunitinib in mouse plasma, brain tumor and normal brain using liquid chromatography-electrospray ionization-tandem mass spectrometry and pharmacokinetic application. *J Pharm Biomed Anal* **51**:958-964.

Footnotes

This study was supported by National Institutes of Health [Grants CA072937 and P50GM071558-03].

Fig. 1. Differential tumor growth rate in sunitinib-treated tumor-bearing animals. U87MG human glioblastoma xenografts were grown subcutaneously in male NIH Swiss nude mice (*nu*/*nu*). Once daily oral administration of vehicle or 40 mg/kg of sunitinib was initiated 14 days after tumor implantation and continued for 30 days. (A) The distribution and median value of the Day-30-to-Day-0 tumor volume ratio in Sunitinib-treated tumor bearing mice (*N* = 21). Sunitinib-treated mice with the Day-30-to-Day-0 tumor volume ratio value being no less than the median value of 4.7 were classified as the sunitinib-resistant animals (*N* = 11), while the rest were defined as the sunitinib-sensitive animals (*N* = 10). (B) Comparison of tumor growth ratio among control, sunitinib-sensitive and -resistant groups. Control animals (N = 5) were sacrificed 16 days after the initiation of the treatment due to their tumors reaching the allowed maximum size (2000 mm^3). $^{++}p < 0.01$ compared with the control group using one-way ANOVA followed by the post-hoc Tukey-Kramer Multiple-Comparison Test. $^{**}p < 0.01$ compared with the sunitinib-sensitive group using the Mann-Whitney U test.

Fig. 2. Quantitation of CD31, α-SMA and NG2 expression in control (N = 5; open column), sunitinib-sensitive (N = 8; horizontal striped column) and sunitinib-resistant (N = 10; solid column) tumors. (A) Results of double fluorescent staining for CD31 and α-SMA; (B) Results of double fluorescent staining for CD31 and NG2; (C) Representative images for the double fluorescent staining of CD31, α-SMA and NG2 in tumor sections from the control, sunitinib-sensitive and -resistant groups. *Columns*, Mean; *bars*, SD. $^{*}p < 0.05$ and $^{++}p < 0.01$ compared with the control group using one-way ANOVA followed by the post-hoc Tukey-Kramer Multiple-Comparison Test.

Fig. 3. Unsupervised hierarchical bi-clustering of the expression patterns of 84 mouse (A) and 84 human (B) angiogenesis associated genes in 5 control tumors (CT), 4 sunitinib-sensitive (ST) tumors and 7 sunitinib-resistant tumors (RT). The color represents relative expression levels where orange represents expression levels greater than the mean for a given gene across all samples whereas blue expression less than the mean. Each colored cell in the heat map represents the gene expression value for a probe in a sample. Principle Component Analysis (PCA) of the mouse (C, mean values, and E, individual animals) and human (D, mean values, and F, individual animals) angiogenesis-associated gene expression was performed to visualize the overall difference in expression levels across samples and groups. The percentage near each axis of the PCA plots denotes the contribution of the principle component to capturing the overall variability within the data. Expression levels of differentially expressed mouse (G) and human (H) angiogenesis-associated genes exhibiting significant difference between the control, sunitinib-sensitive and –resistant groups ($P < 0.05$ compared with the control) are visualized as a bi-clustering heatmap using the same color scheme and normalization procedure as in A and B.

Fig. 4. Phosphorylated protein kinases and other kinase substrates protein expression levels in sunitinib-sensitive (A) and –resistant tumors (B) compared with control tumors. Upregulation: A protein expression ratio of the sunitinib-treated tumor to the control tumor being ≥ 1.5. Downregulation: A protein expression ratio of the control tumor to the sunitinib-treated tumor being ≥ 1.5. Network created from up- (C) and down-regulated (D) kinases and other phospho-proteins. Links denote activation (arrowheads) and inhibition (ball-head); dashed arrows represent indirect effects; nodes are color coded by up-regulated (red), down-regulated (blue) and unchanged (light gray); additional nodes that were not measured are color coded in dark

gray. Links are marked based on their database sources whereas numbers represent PubMed IDs.

Fig. 5. Modulated expression levels of ABCG2 and selected phosphorylated and total kinases in sunitinib-sensitive and –resistant tumors. (A) Western blot analysis of ABCG2 levels in untreated (*N* = 4), sunitinib-sensitive (*N* = 6) and –resistant (*N* = 4) tumors. Anti-β-actin immunoblot is shown as an independent loading control. (B) Western blot analysis of phosphorylated and total c-Jun, ERK1/2, GSK3α/β and PLCγ1 in untreated, sunitinib-sensitive [S] and –resistant [R] tumors. $S^{\S}$ - Sample was not included in the study due to the missing dose on Day 30. (C) Quantitation of Western blotting results using densitometric analysis. The results are plotted as percent of control. *Columns*, Mean; *bars*, SD. Open column, control group; horizontal striped column, sunitinib-sensitive group; solid column, sunitinib-resistant group. $^{*}p < 0.05$ compared with the control group using one-way ANOVA followed by the post-hoc Tukey-Kramer Multiple-Comparison Test. $^{+}p < 0.05$ compared with the sunitinib-sensitive group using one-way ANOVA followed by the post-hoc Tukey-Kramer Multiple-Comparison Test.

Table 1. Unbound sunitinib systemic and tumor exposure in sunitinib-sensitive and –resistant tumors

Groups	**Unbound Tumor IF AUC_{0-24} (ng*h/ml)**	**Unbound Plasma AUC_{0-24} (ng*h/ml)**	**Unbound Tumor IF/Plasma AUC Ratio**
Sensitive Tumor (*N* = 6)	881.0 ± 682.1	548.6 ± 178.4	1.93 ± 1.70
Resistant Tumor (*N* = 4)	871.8 ± 268.7	405.2 ± 158.9	2.30 ± 0.79
***p*-values**	0.594	0.166	0.594

Table 2. Tumor angiogenesis in control, sunitinib-sensitive and –resistant tumors.

Groups	CD31/α-SMA Double Staining			CD31/NG2 Double Staining		
	MVD (%)	**α-SMA Density (%)**	**Vessel maturity**	**MVD (%)**	**NG2 Density (%)**	**Pericyte recruitment**
Control	7.49 ± 2.06	2.05 ± 0.75	8.49 ± 3.09	8.91 ± 1.39	3.08 ± 1.14	18.39 ± 3.08
Sensitive	1.88 ± 0.55 **	1.28 ± 0.47	27.95 ± 10.37 **	1.86 ± 0.51**	0.64 ± 0.16 **	7.85 ± 5.93 *
Resistant	1.81 ± 0.47 **	1.18 ± 0.64	25.17 ± 9.56 *	1.52 ± 0.26 **	0.43 ± 0.12 **	9.88 ± 5.72 *

*$p < 0.05$, ** $p < 0.01$ compared with control using one-way ANOVA and Tukey-Kramer Multiple-Comparison Test.

Fig. 1A

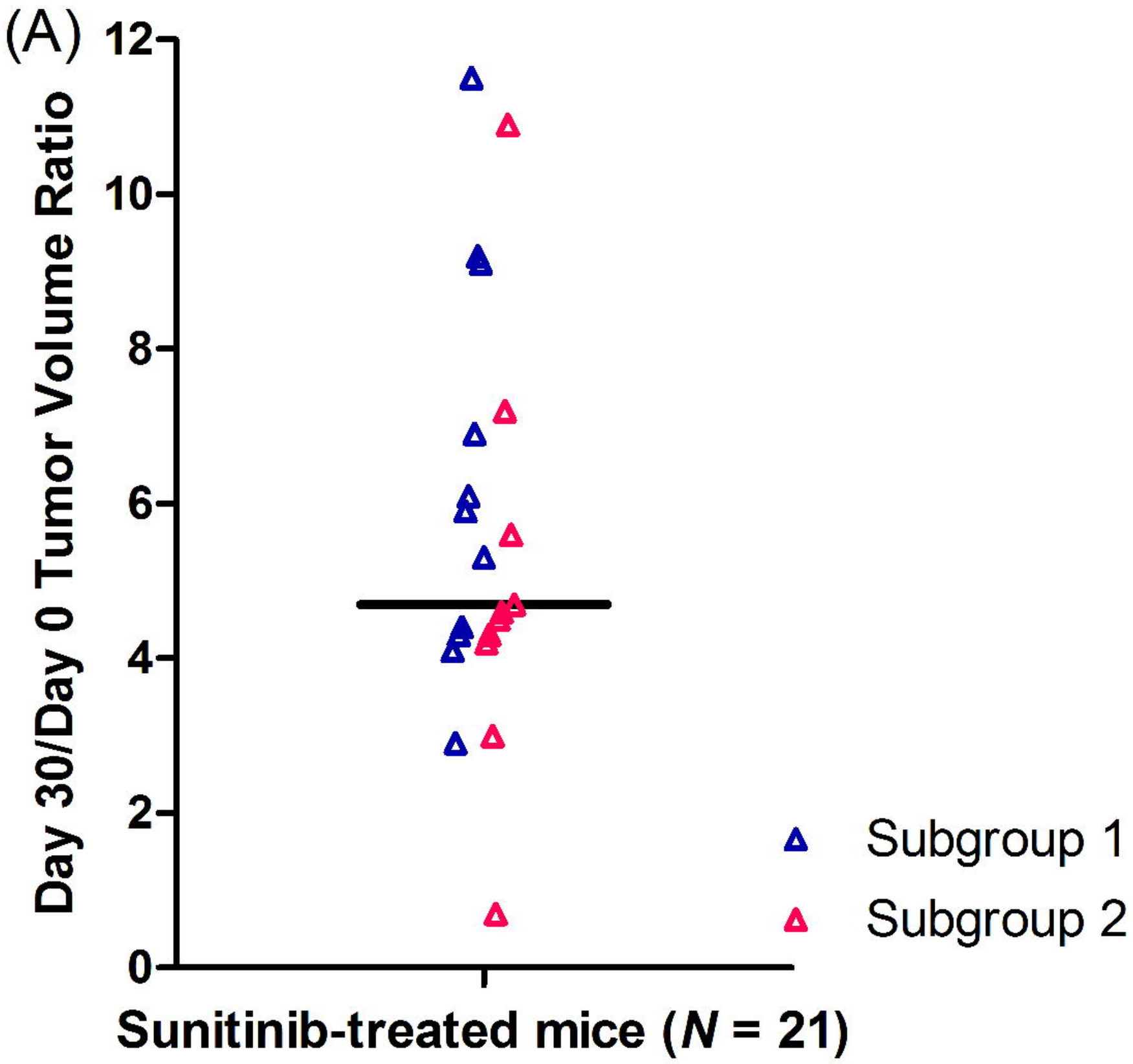
(A)
12
10
8
6
4
2
0
Day 30/Day 0 Tumor Volume Ratio
Subgroup 1
Subgroup 2
Sunitinib-treated mice (N = 21)

Fig. 1B

(B)

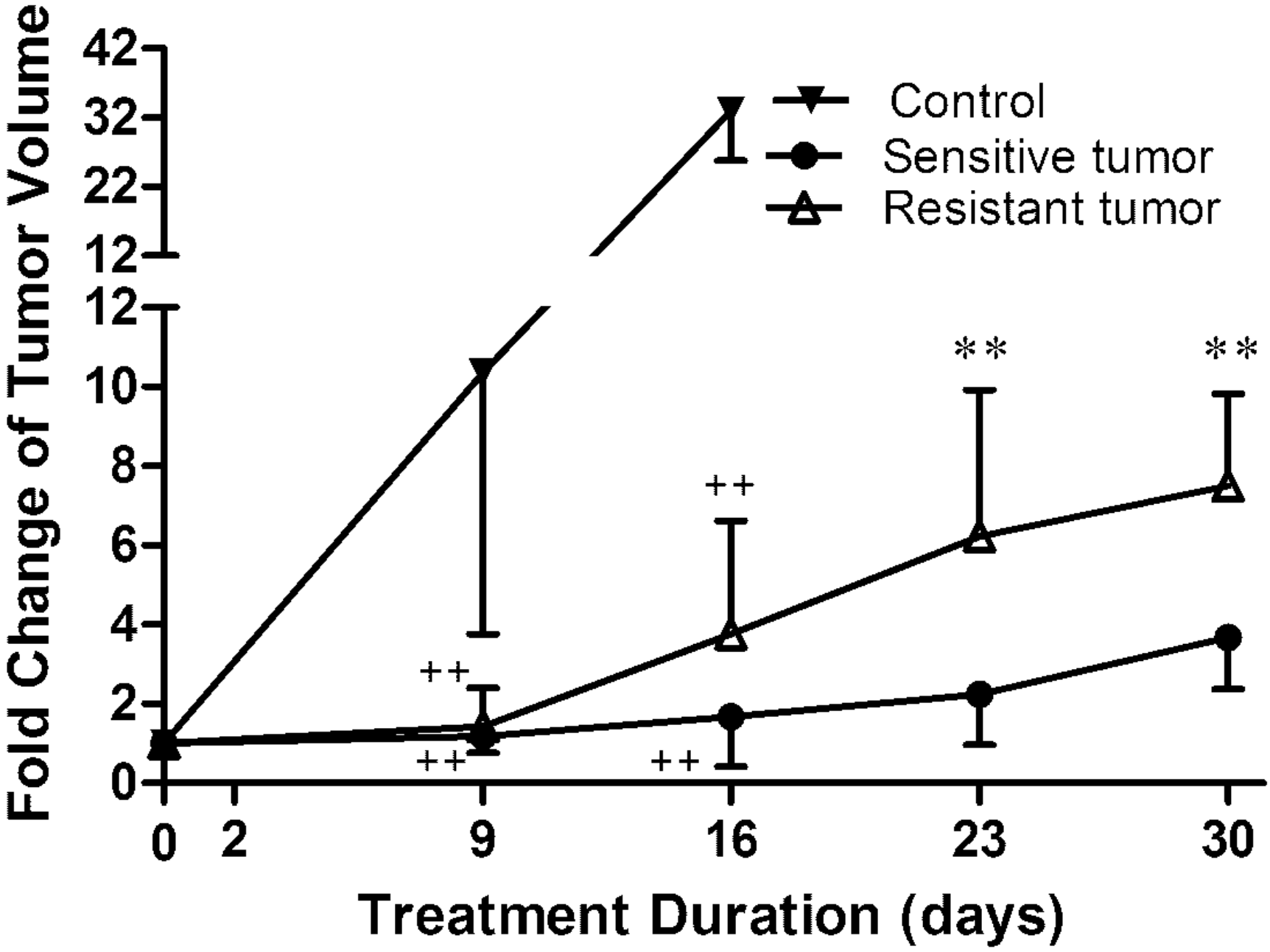
Fold Change of Tumor Volume
42
32
22
12
12
10
8
6
4
2
0
Control
Sensitive tumor
Resistant tumor
**
**
++
++
++
0
2
9
16
23
30
Treatment Duration (days)

Fig. 2A

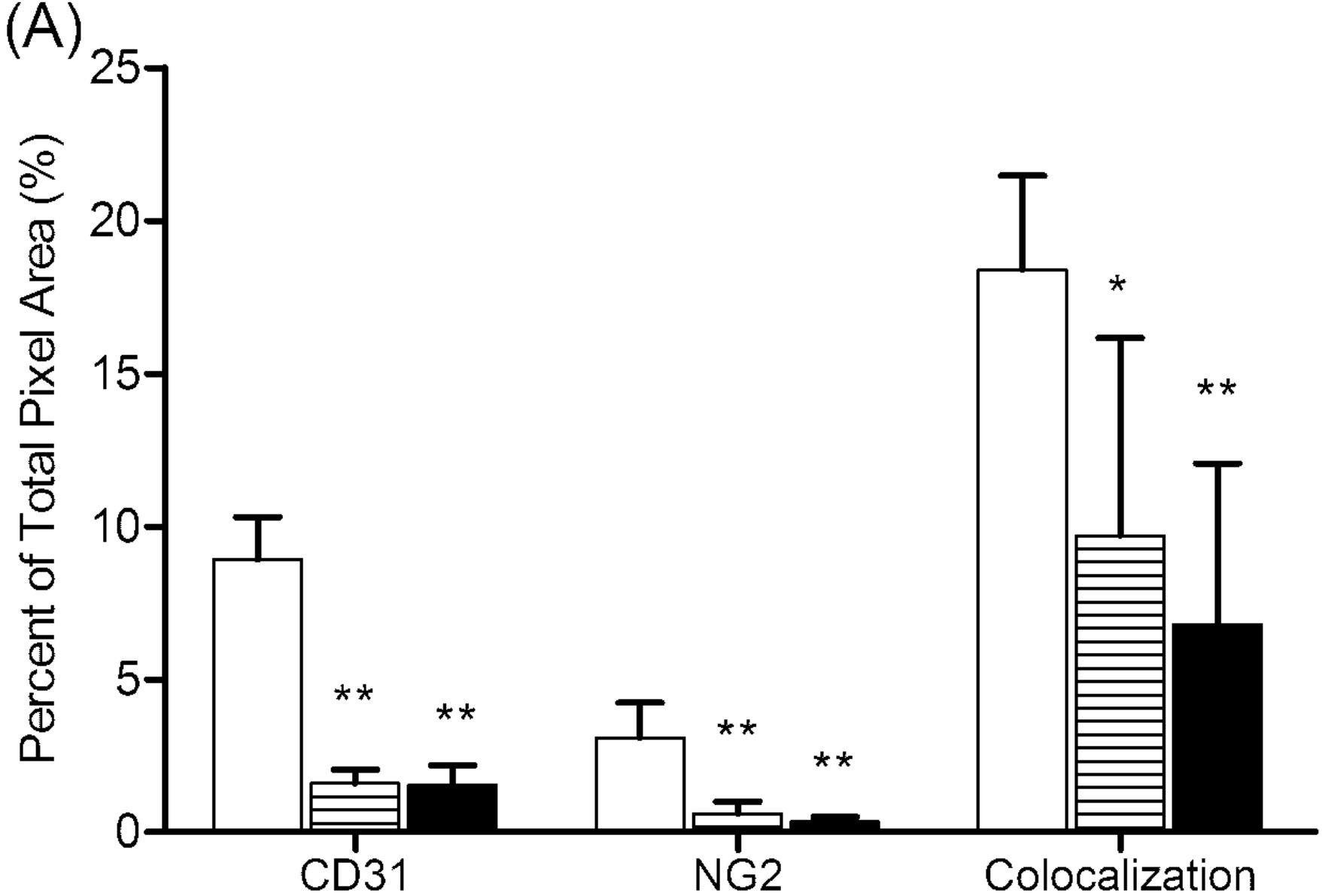
(A)
Percent of Total Pixel Area (%)
25
20
15
10
5
0
**
**
**
**
*
**
CD31
NG2
Colocalization

Fig. 2B

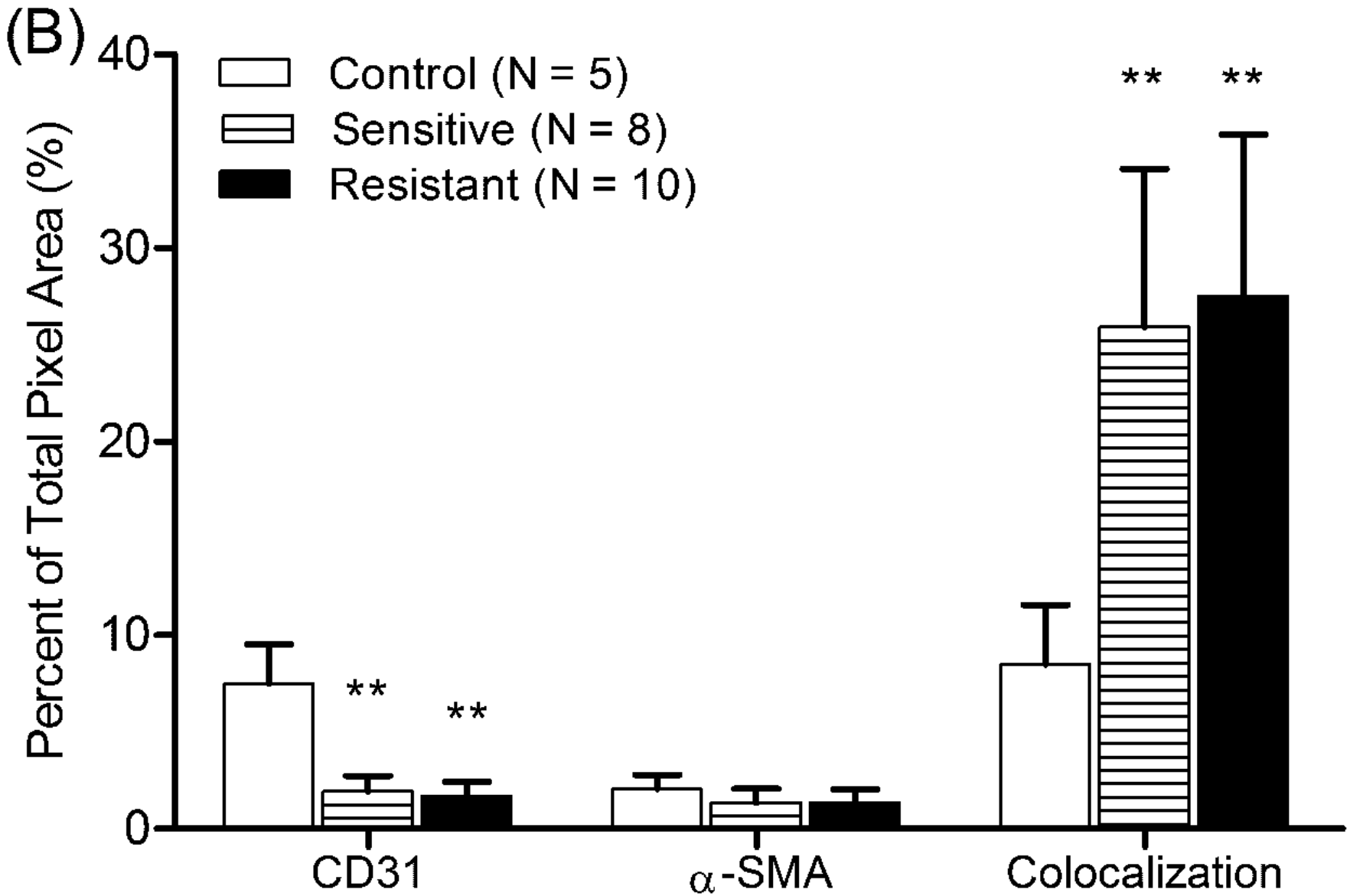
(B)
Control (N = 5)
Sensitive (N = 8)
Resistant (N = 10)
Percent of Total Pixel Area (%)
40
30
20
10
0
**
**
**
**
CD31
α-SMA
Colocalization

Fig. 2C

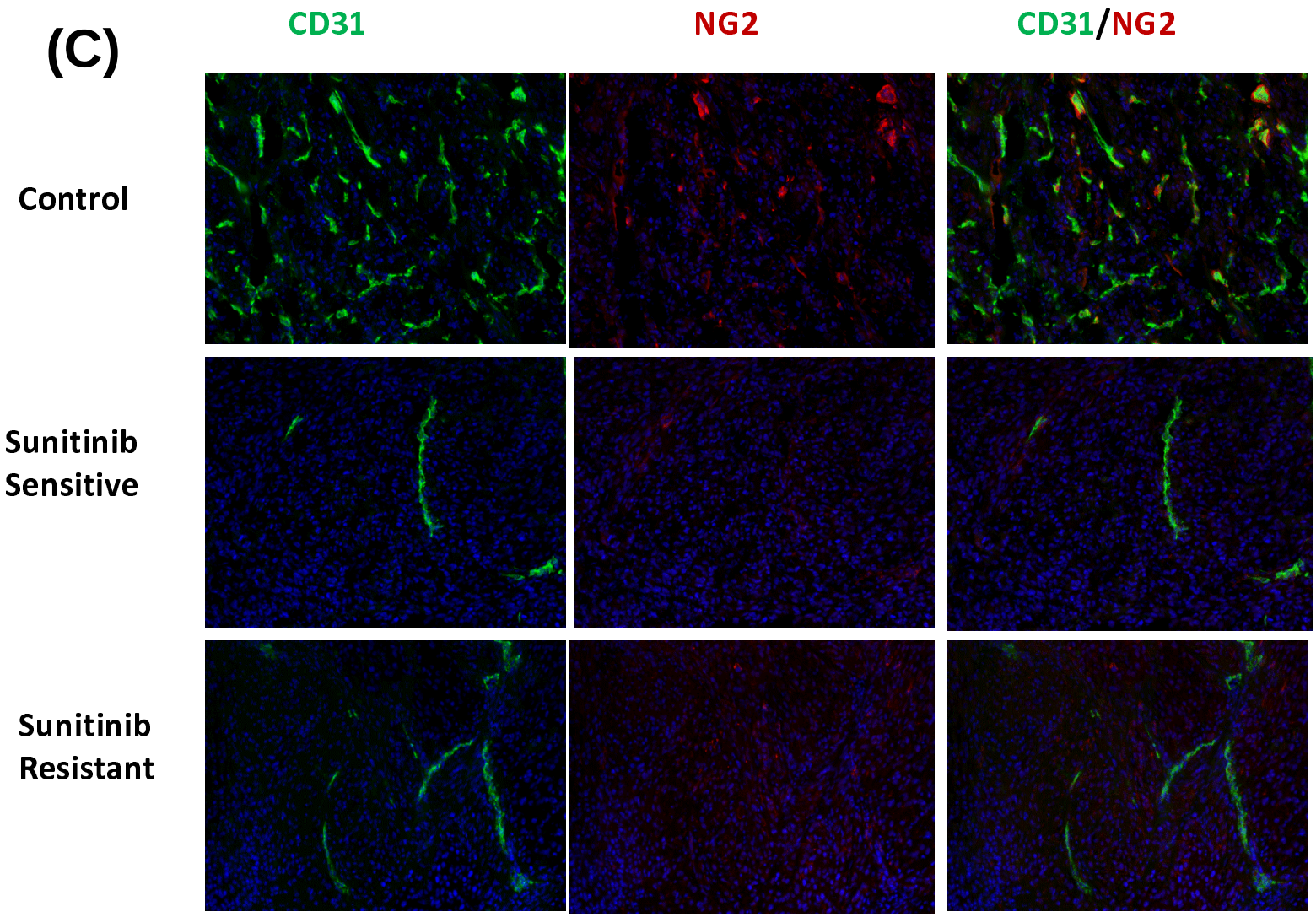
(C)
CD31
NG2
CD31/NG2
Control
Sunitinib Sensitive
Sunitinib Resistant

Fig. 2D

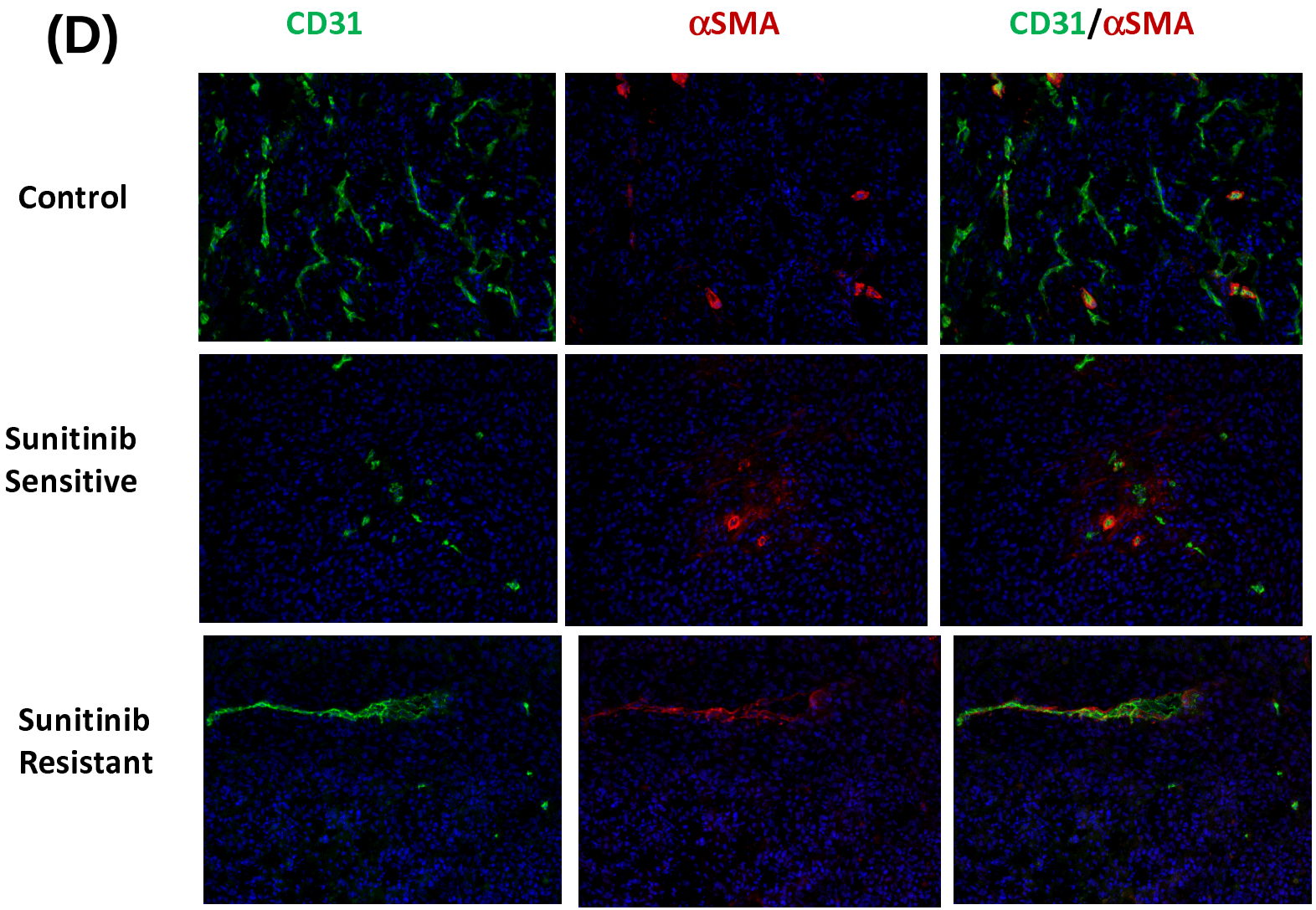
(D)
CD31
αSMA
CD31/αSMA
Control
Sunitinib Sensitive
Sunitinib Resistant

Fig. 3A – 3B

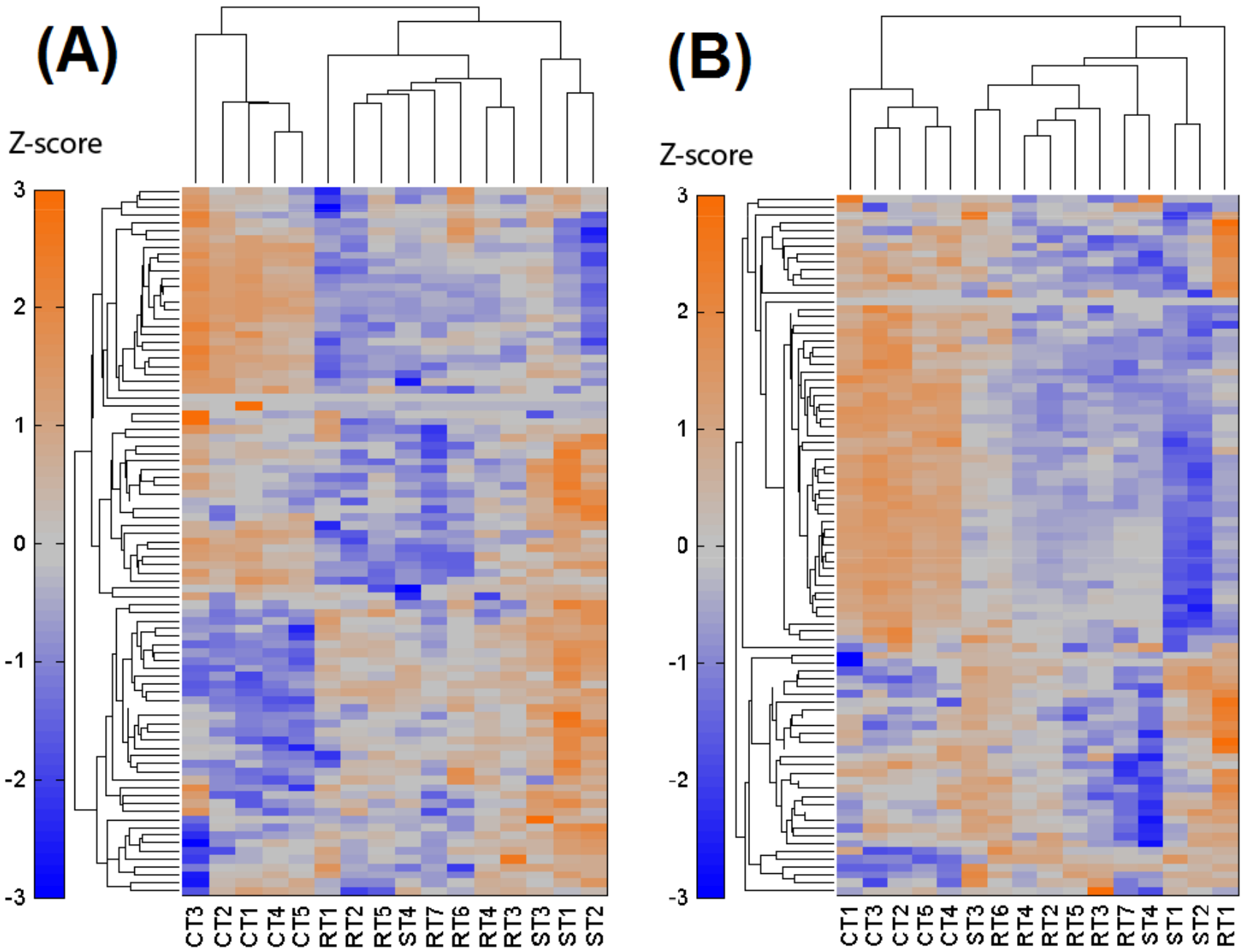
(A)
Z-score
3
2
1
0
-1
-2
-3
CT3
CT2
CT1
CT4
CT5
RT1
RT2
RT5
ST4
RT7
RT6
RT4
RT3
ST3
ST1
ST2
(B)
Z-score
3
2
1
0
-1
-2
-3
CT1
CT3
CT2
CT5
CT4
ST3
RT6
RT4
RT2
RT5
RT3
RT7
ST4
ST1
ST2
RT1

Fig. 3C – 3D

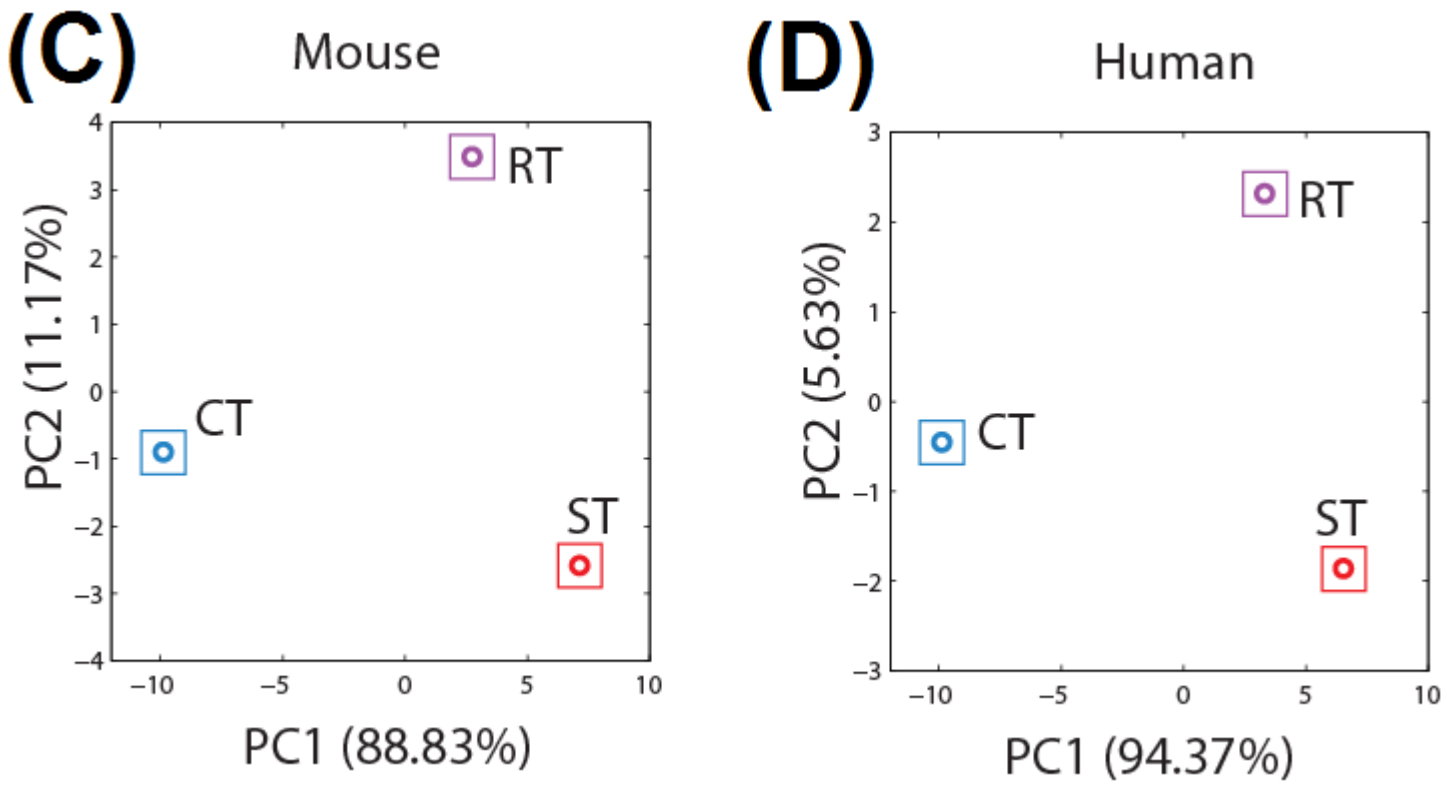
(C)
Mouse
RT
CT
ST
PC2 (11.17%)
PC1 (88.83%)
4
3
2
1
0
−1
−2
−3
−4
−10
−5
0
5
10
(D)
Human
RT
CT
ST
PC2 (5.63%)
PC1 (94.37%)
3
2
1
0
−1
−2
−3
−10
−5
0
5
10

Fig. 3E – 3F

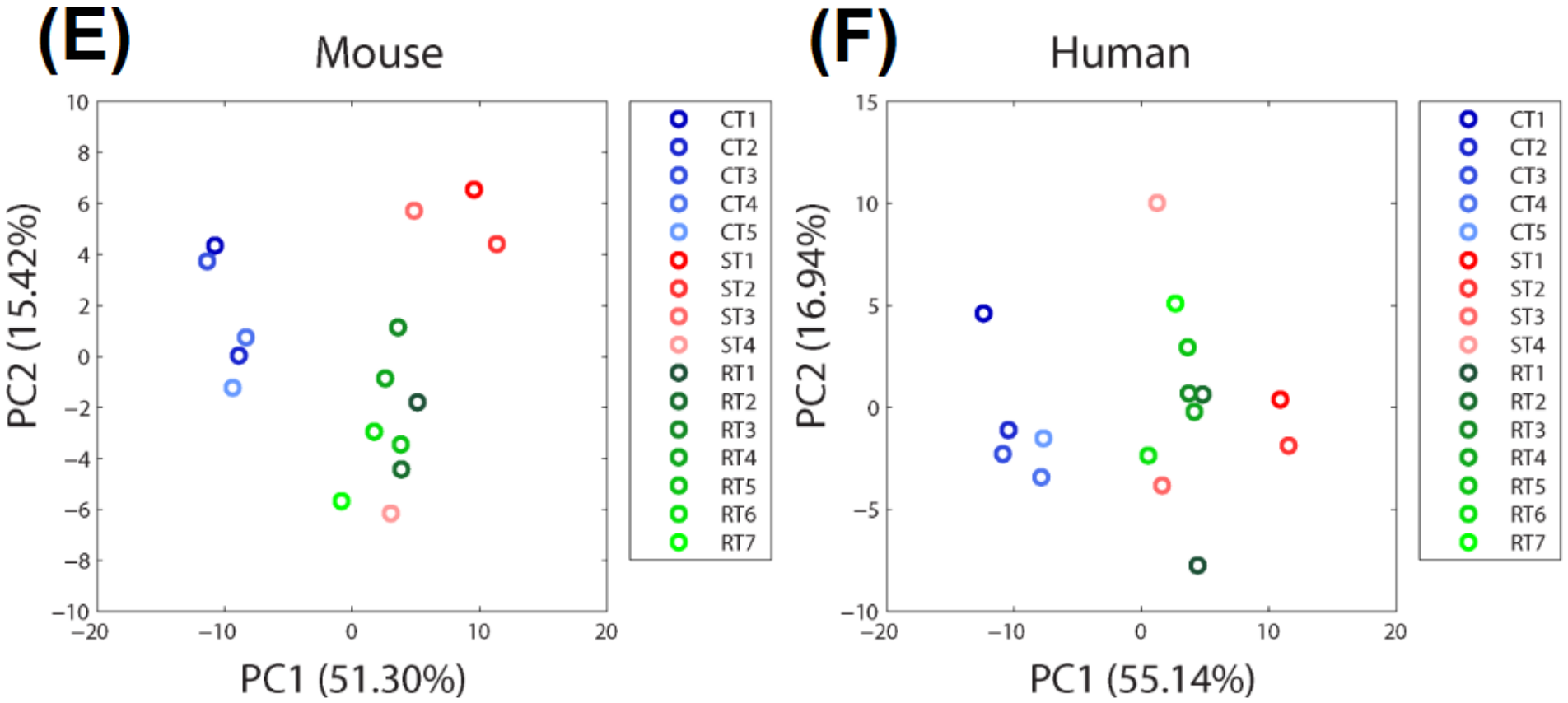
(E)
Mouse
PC2 (15.42%)
PC1 (51.30%)
(F)
Human
PC2 (16.94%)
PC1 (55.14%)
CT1
CT2
CT3
CT4
CT5
ST1
ST2
ST3
ST4
RT1
RT2
RT3
RT4
RT5
RT6
RT7

Fig. 3G – 3H

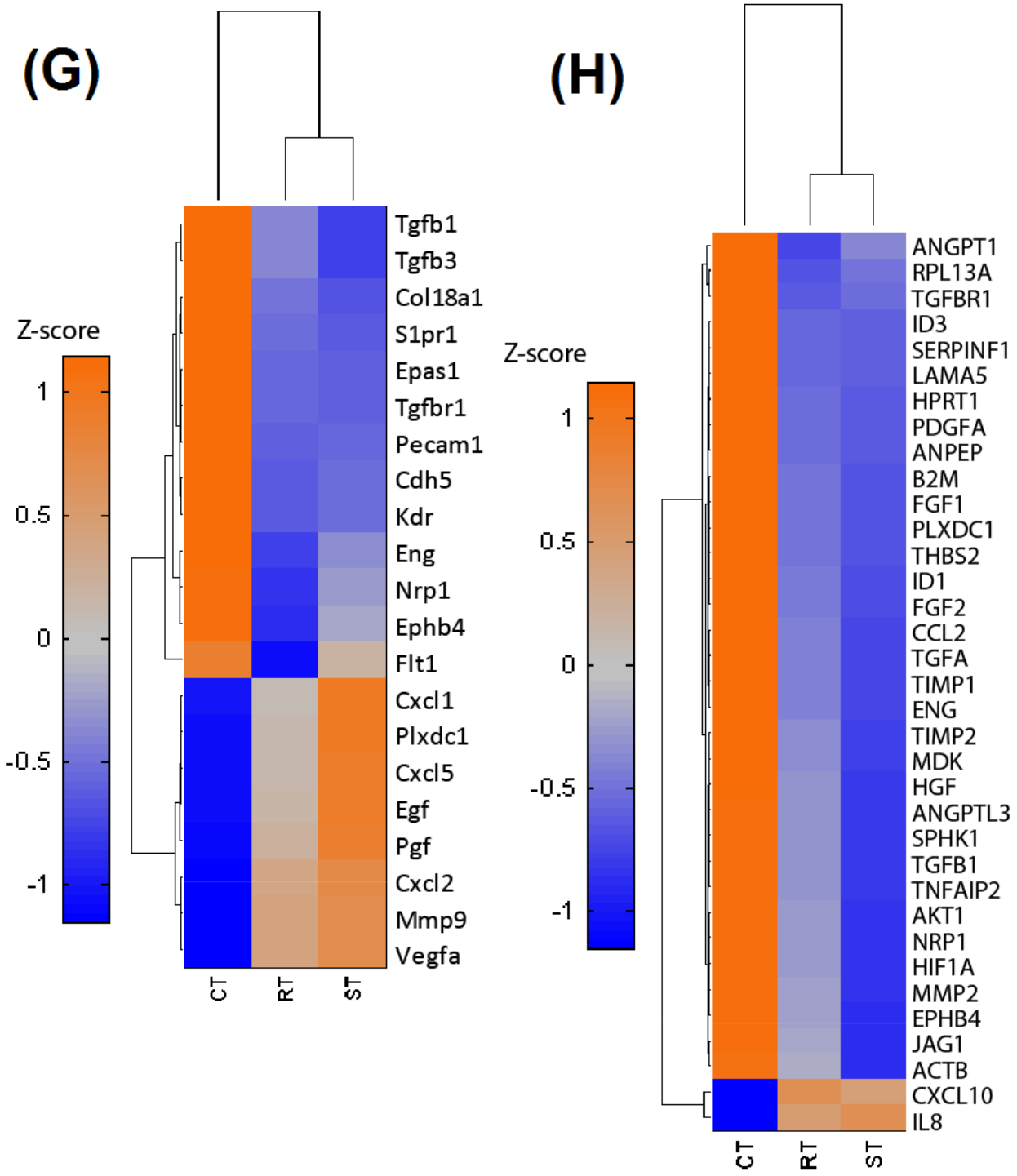
(G)
Z-score
1
0.5
0
-0.5
-1
Tgfb1
Tgfb3
Col18a1
S1pr1
Epas1
Tgfbr1
Pecam1
Cdh5
Kdr
Eng
Nrp1
Ephb4
Flt1
Cxcl1
Plxdc1
Cxcl5
Egf
Pgf
Cxcl2
Mmp9
Vegfa
CT
RT
ST
(H)
Z-score
1
0.5
0
-0.5
-1
ANGPT1
RPL13A
TGFBR1
ID3
SERPINF1
LAMA5
HPRT1
PDGFA
ANPEP
B2M
FGF1
PLXDC1
THBS2
ID1
FGF2
CCL2
TGFA
TIMP1
ENG
TIMP2
MDK
HGF
ANGPTL3
SPHK1
TGFB1
TNFAIP2
AKT1
NRP1
HIF1A
MMP2
EPHB4
JAG1
ACTB
CXCL10
IL8
CT
RT
ST

Fig. 4A

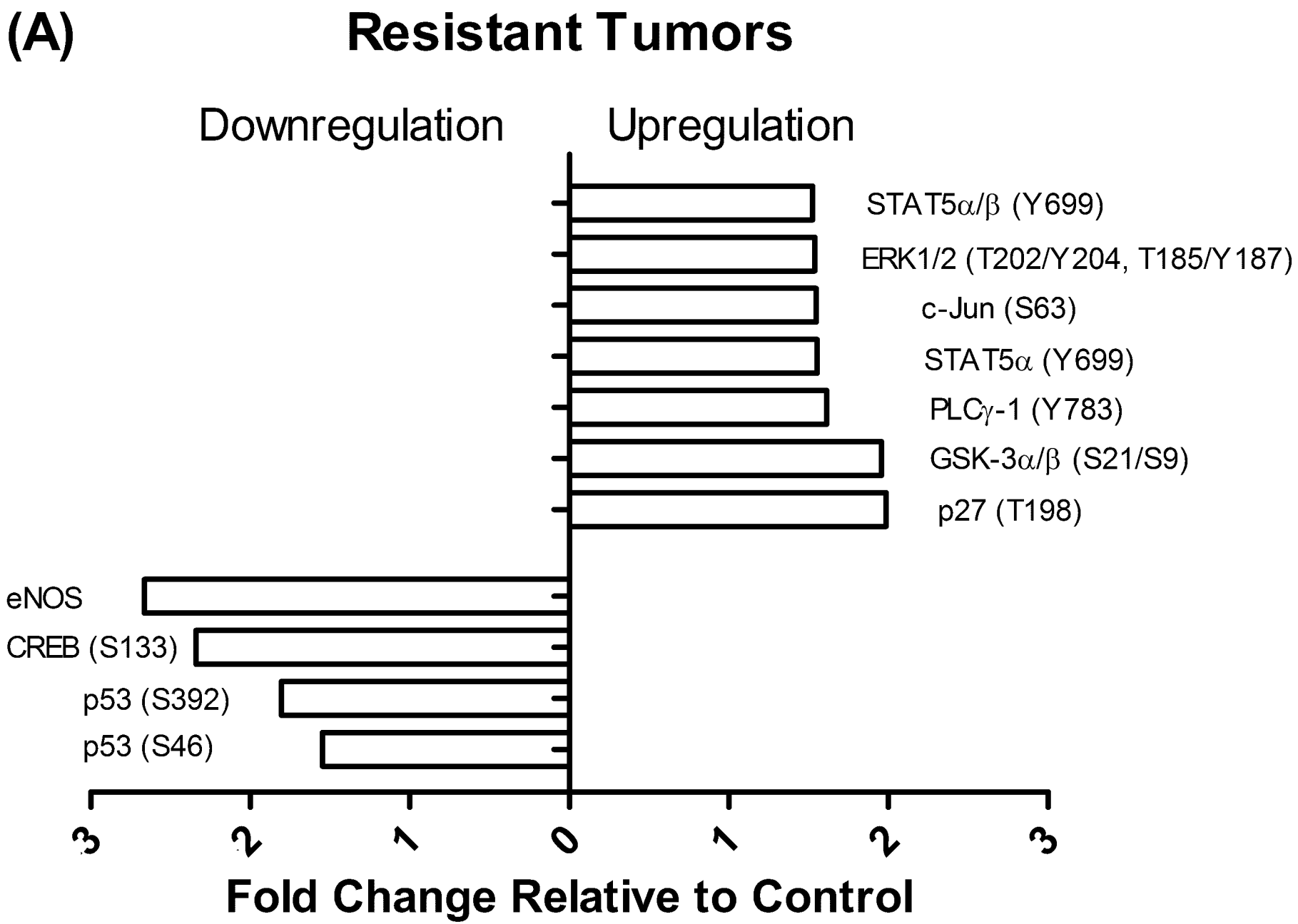
(A)
Resistant Tumors
Downregulation
Upregulation
STAT5α/β (Y699)
ERK1/2 (T202/Y204, T185/Y187)
c-Jun (S63)
STAT5α (Y699)
PLCγ-1 (Y783)
GSK-3α/β (S21/S9)
p27 (T198)
eNOS
CREB (S133)
p53 (S392)
p53 (S46)
3
2
1
0
1
2
3
Fold Change Relative to Control

Fig. 4B

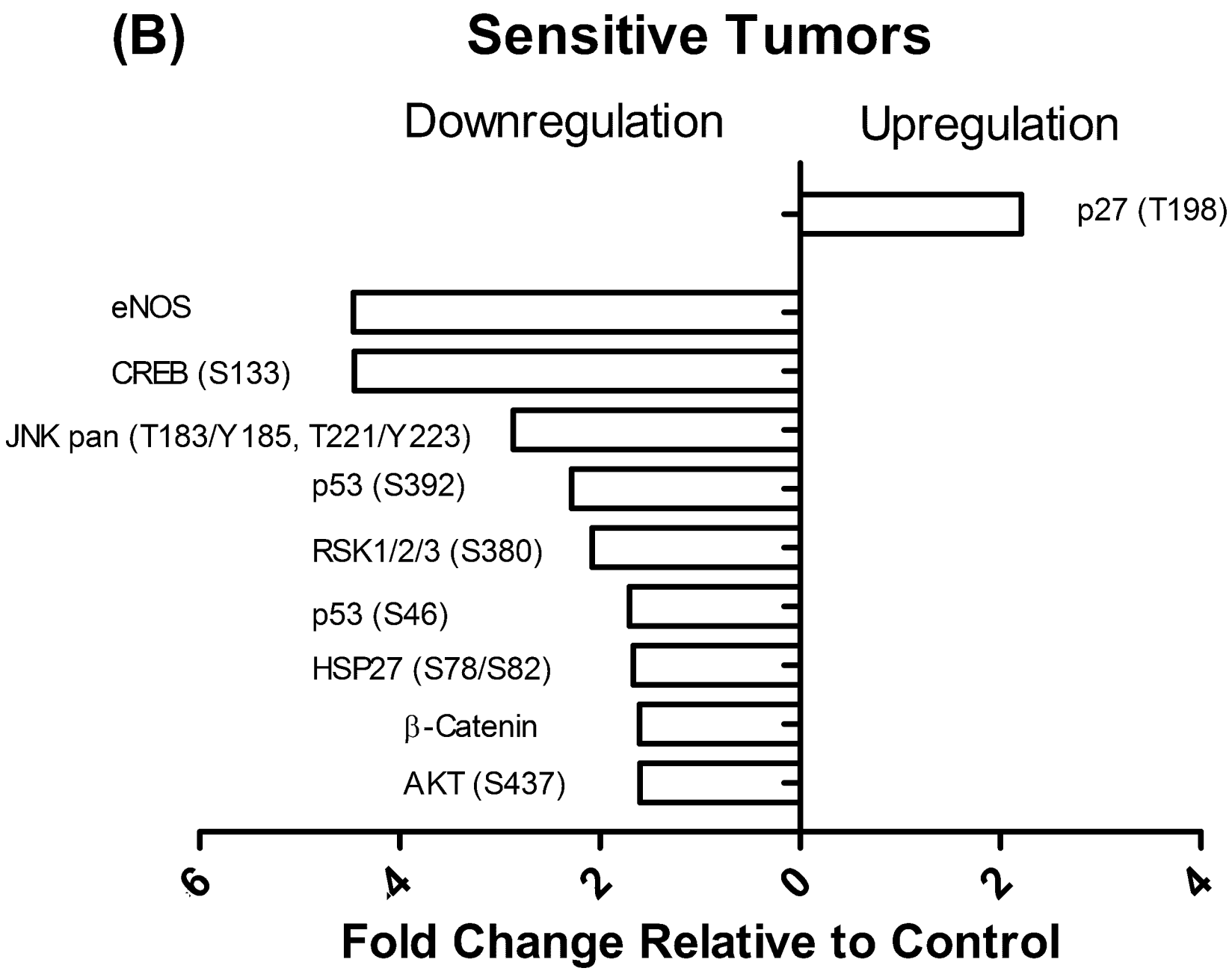
(B)
Sensitive Tumors
Downregulation
Upregulation
p27 (T198)
eNOS
CREB (S133)
JNK pan (T183/Y185, T221/Y223)
p53 (S392)
RSK1/2/3 (S380)
p53 (S46)
HSP27 (S78/S82)
β-Catenin
AKT (S437)
6
4
2
0
2
4
Fold Change Relative to Control

Fig. 4C

(C)

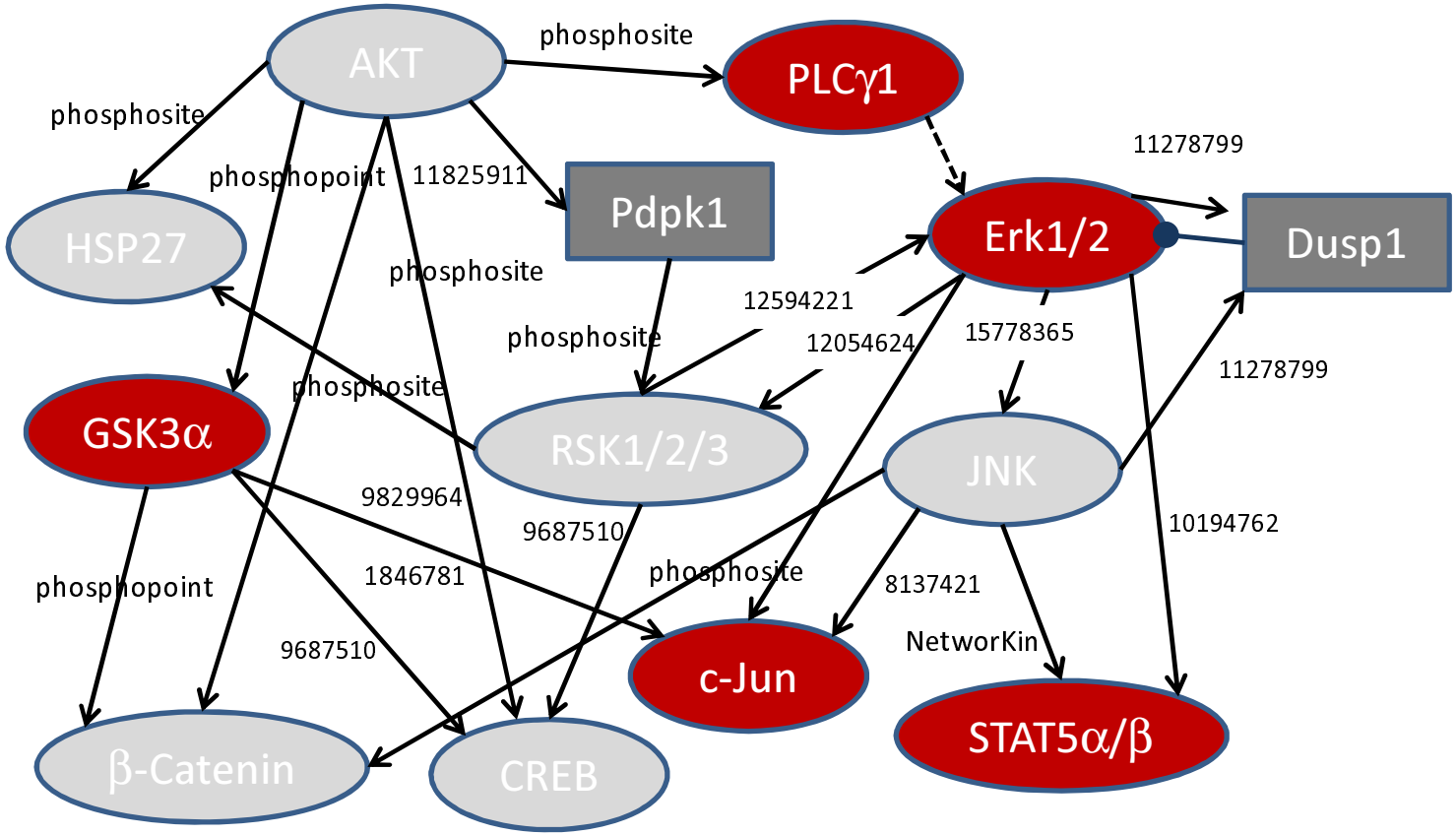
AKT
phosphosite
PLCγ1
phosphosite
phosphopoint
11825911
Pdpk1
11278799
HSP27
Erk1/2
Dusp1
phosphosite
12594221
phosphosite
12054624
15778365
11278799
phosphosite
GSK3α
RSK1/2/3
JNK
9829964
9687510
10194762
phosphopoint
1846781
phosphosite
8137421
9687510
NetworKin
c-Jun
β-Catenin
CREB
STAT5α/β

Fig. 4D

(D)

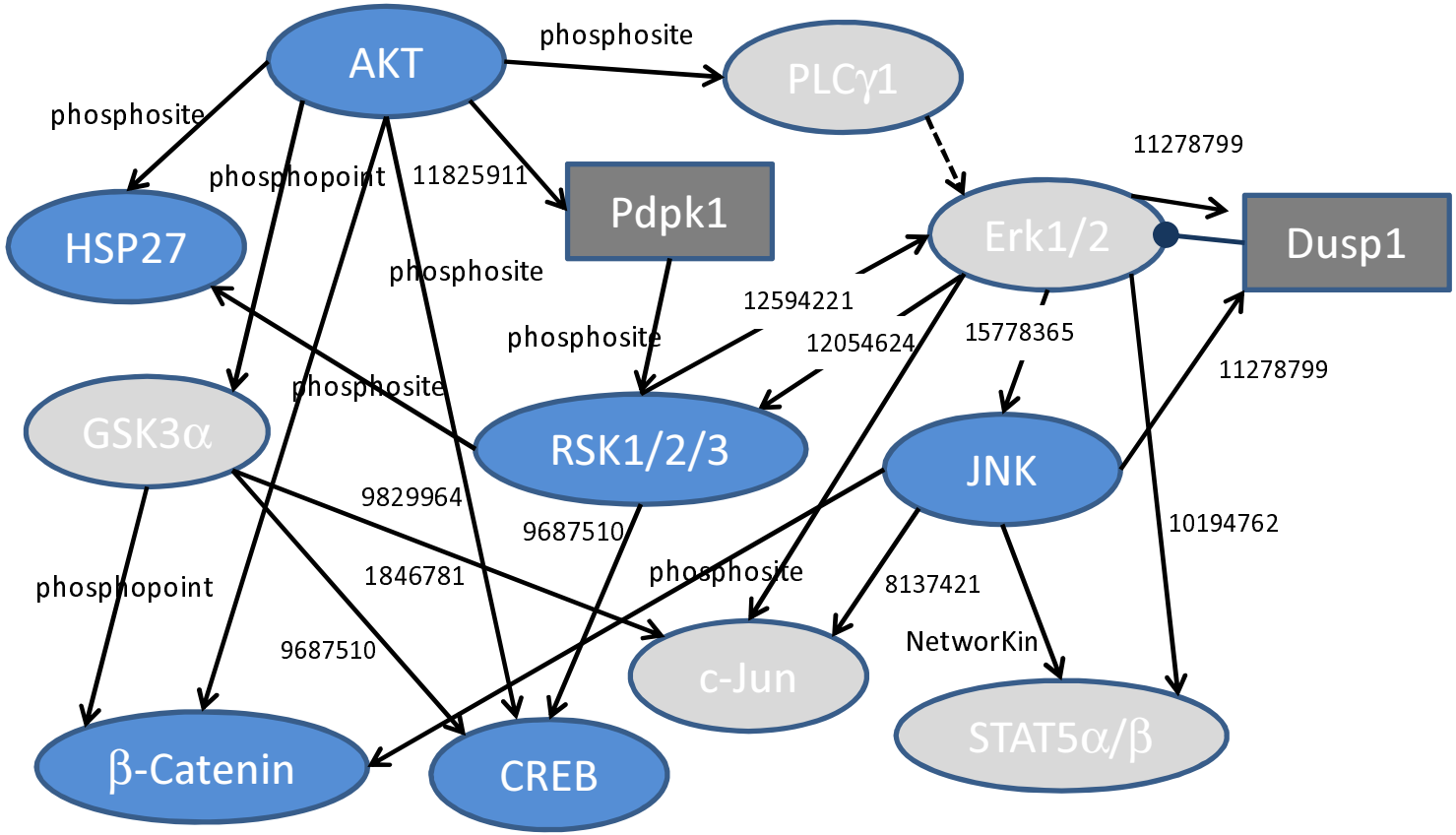
AKT
phosphosite
PLCγ1
phosphosite
phosphopoint
11825911
Pdpk1
11278799
HSP27
Erk1/2
Dusp1
phosphosite
12594221
phosphosite
12054624
15778365
11278799
phosphosite
GSK3α
RSK1/2/3
JNK
9829964
9687510
10194762
phosphopoint
1846781
phosphosite
8137421
NetworKin
9687510
c-Jun
β-Catenin
CREB
STAT5α/β

Fig. 5A – 5C

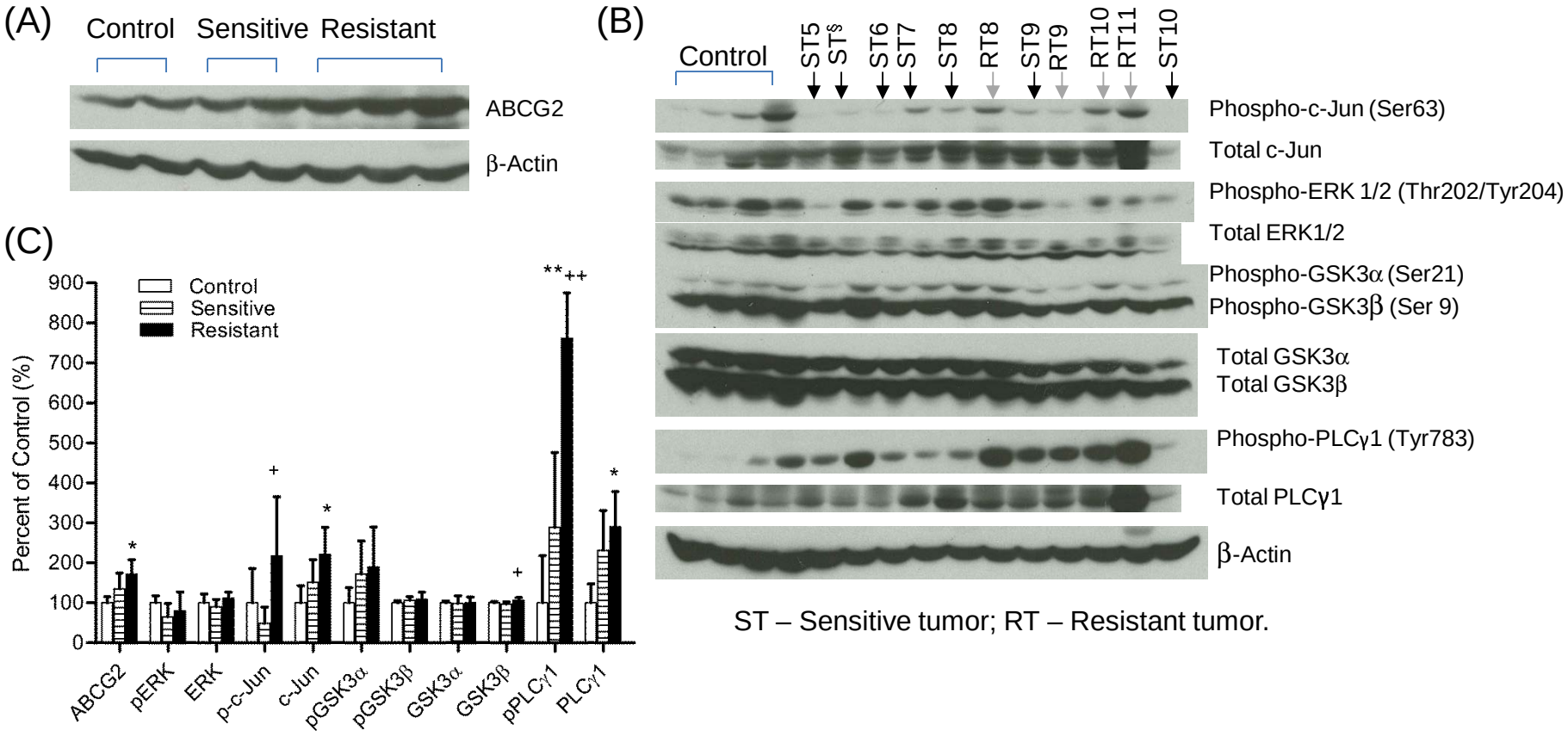

ST – Sensitive tumor; RT – Resistant tumor.